

## Topic 4.3

### STRUCTURE CHANGE FORECASTING

Rapporteur: Chris Fogarty  
Canadian Hurricane Center  
45 Alderney Drive, Dartmouth, NS  
Canada, B2Y 2N6  
Email: chris.fogarty@ec.gc.ca  
Phone: +902-426-9181

Rapporteur: Fuqing Zhang  
Department of Meteorology  
Pennsylvania State University  
University Park, PA, USA  
ZIP 16802  
Email: fzhang@psu.edu  
Phone: +814-865-0470

Working group: (see Excel file)

**Abstract:** In this section we provide a summary of recent research and the state of forecasting the structure of tropical cyclones worldwide from their early stage during formation, to the latter stages of extratropical transition. Not unlike overall intensity prediction, forecasting the three-dimensional structure of the tropical cyclone is very challenging, with size (wind field) prediction in its relative infancy. The ability to anticipate changes in the storm's size, for example, fundamentally lies in accurate measurements of the storm structure. Aircraft and dropsonde data assist in this regard as well as remote sensing by satellites. Trends in the variables measured through these means often serve as a short-term predictor for changes in the storm's structure and for input into data assimilation schemes of numerical weather models.

#### 4.3.0 Introduction

This section of the report will begin with a summary of diagnostic and forecasting topics related to storm structure followed by a summary of recent research with respect to NWP development and we'll present some aspects of data assimilation and verification.

#### 4.3.1 Vertical motion in the lower troposphere and relation to intensity change

We first take a look at some operational diagnostics from Australia (Callaghan and ... 2014). The Brisbane Tropical Cyclone Warning Centre has used two forms of a thermal advection diagnostic to identify relatively large areas of isentropic ascent and descent for many years. When the thermodynamic conditions are favourable, the ascent regions are correlated with significant outbreaks of convection that produce heavy rainfall. The diagnostic is based on the relationship between geostrophic winds that turn with height and flow perpendicular to thickness contours within the circulation of the TC. As the relationship is also valid for the more general case of gradient winds, the diagnostic, in theory, should be useful for most heavy-rain-bearing tropical systems. The diagnostics applied to numerical weather prediction models are valuable forecast tools as they identify heavy rainfall threat regions within which the extreme rain is likely to fall, whereas the rainfall from the same models is often under predicted or has large location errors.

Applied to TCs, the diagnostics have been used successfully to forecast storm formation, rapid intensification and decay.

It has been found that in the northern Australian region since 2003 all intensifying tropical lows and tropical cyclones did so in the presence of moderate 850 to 500 hPa shear (Brisbane Tropical Cyclone Warning Centre, unpublished Study), which will be associated with horizontal thermal gradients if the flow is in near-gradient wind balance and the shear includes directional variation.

An example of the diagnostic applied to a case of rapid tropical cyclone intensification in European Centre for Medium-Range Weather Forecast (EC) analyses is shown in Figure 1 for severe TC Yasi just before landfall. In a general sense the numerical models forecast the intensification of Yasi as it moved westward across the Coral Sea towards Australia. At the time in Figure 1 Yasi was intensifying from an Australian Category 4 tropical cyclone to a Category 5 TC. Yasi made landfall two and a half hours after this analysis. CAA and descent is indicated within the dotted black line and WAA and ascent is indicated outside this line. Note the strong 700 hPa flow onto the coast south of the circulation which was flowing across strong shears (red arrows) indicating strong warm air advection. The heaviest rain was recorded in this zone extending northwards up to the centre of the circulation. Typically this pattern favours rapid intensification when the WAA has a larger areal extent than the CAA. Such thermal advection distributions associated with TC intensification are common in all global TC basins but application of this diagnostic has yet to be applied in a broader sense.

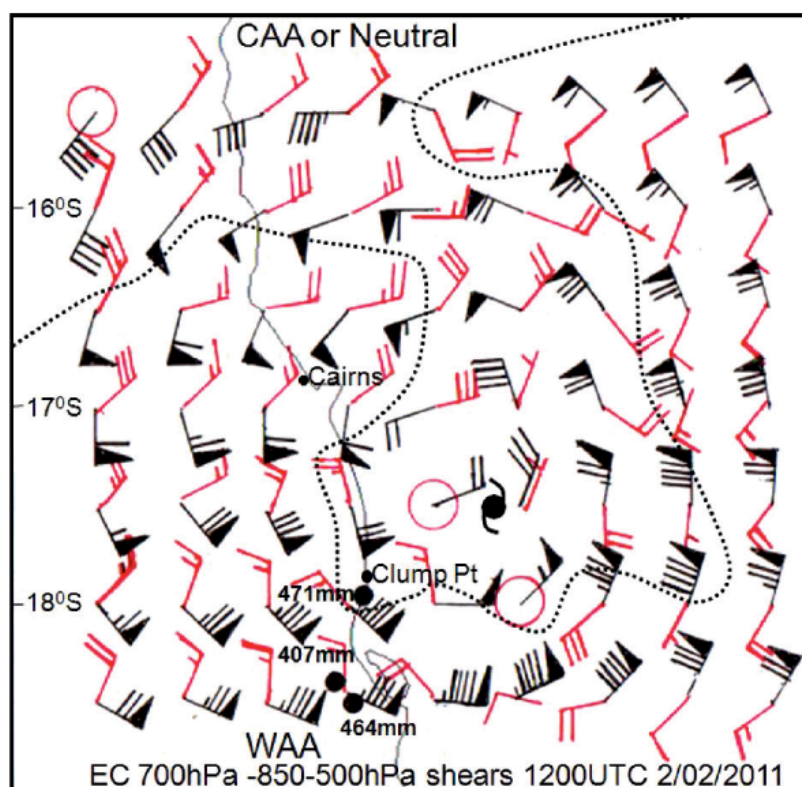


Figure 1. EC 700 hPa wind barbs (black) and 850 to 500 hPa shear vectors (red) for TC Yasi at 1200 UTC 2 February 2011 (cyclone symbol denotes actual sea level position at that time). The three largest rainfall reports in the 24 hour to 2300 UTC 2 February 2011 are plotted south of Clump Point which was the place of landfall at 1400 UTC 2 February 2011. The warm air advection region lies in the area outside the dotted black line while the cold air advection or neutral region is enclosed by the dotted black line.

### 4.3.2 Wind field asymmetry during ET in the West Pacific

Probabilistic risk assessment systems for tropical cyclone hazard rely on large ensembles of model simulations to characterize cyclone tracks, intensities and the extent of the associated damaging winds. Given computational costs the wind field is often modelled using parametric formulations that make assumptions based on observations of tropical systems (e.g. satellite, aircraft reconnaissance). In particular most of the damaging contribution is assumed right of the moving cyclone with the left hand side winds much weaker due to the storm motion direction.

In a study using JRA-25 reanalysis data Kitabatake (2011) estimated that 40 % of WNP cyclones experience extratropical transition. Given the country's meridional extent and location within the Pacific basin, Japan, which represents the main area of exposure for the western North Pacific (WNP), is particularly influenced by such transitioning systems. From a risk assessment point of view it is critical to assess whether or not tropical wind models are suitable to represent the associated wind fields. In particular, the validity of the asymmetry assumption is questionable as historical events such as Tokage in 2004 have highlighted the potential for damaging winds on both sides of a storm track while Fujibe and Kitabatake (2007) and later Kitabatake and Fujibe (2009) showed such types of wind fields are common for cyclones transitioning around Japan

Using 31 years of data from the Climate Forecast System Reanalysis (CFSR; Saha et al., 2010) product Loridan et al. (2014a) analysed the relative magnitude of wind speeds on both sides of the cyclones' tracks. Figure 2 shows peak winds on the right ( $V_{\max.rhs}$ ) and left ( $V_{\max.lhs}$ ) hand sides of the track heading direction, computed within a 800 km x 800 km box centred on the cyclone. Note  $V_{\max.lhs}$  is recorded at least 100 km left of the track (see Loridan et al. 2014a for details). For the purpose of Figure 2, the cyclones are split in two groups using the IBTrACS end of transition time stamp information: (1) tropical cases are characterized by all 6 hourly snapshots that are at least 96 h before the cyclone is flagged as ET (Figure 2a) and (2) transitioning/ET cases by all snapshots that are 24 h before the flag or later (Figure 2b). The distinct behavior is obvious with the majority of points below the 1:1 line in the tropical case (Figure 2a) while the magnitude of the winds on both sides of the track is much more similar for transitioning/ET cases (Figure 2b). Most importantly for risk assessment applications, stronger winds are often observed left of the track in the transitioning/ET case, especially for the largest values recorded (e.g.  $> 35 \text{ m s}^{-1}$ ).

From a classification of cyclones in terms of their most frequent wind patterns this study shows that for 2/3 of cases that transition around Japan the asymmetry assumption is not valid. These "left hand side contribution" (LHSC) wind fields exhibit strong winds on both sides of the moving cyclone with the maximum magnitude located either to the right or to the left in a pattern often described as a "horseshoe". A first order analysis of cyclone characteristics 12 h before it completes its transition highlights some potential predictors for the likelihood of a LHSC case. They can be primarily characterized as more likely in autumn, and having more intense maximum winds. The importance of the relative position of the cyclone and the jet stream during transitioning is discussed briefly but should be further investigated to better characterize the conditions favourable to these LHSC cases. This has some potential to determine when a new "horseshoe" model should be used. For the other 1/3 of cases tropical formulations are applicable, provided they are calibrated accordingly.

In a follow up study (Loridan et al. 2014b), a new parametric formulation specifically designed for the transitioning phase is introduced. It is based on a limited amount of input parameters and uses a parametric bias correction field to achieve the wind target shape. Calibration of the proposed model against 37 WRF simulations of transitioning WNP cyclones leads to a set of three formulations that cover the range of observed transitioning wind fields. First

results reveal the potential of the method to replicate the features specific to the transition phase (Figure 3), such as a wide extent of damaging winds on both sides of the cyclone track with a maximum wind magnitude that can be located on either side. The extent to which the change in wind field pattern during transitioning impacts the modelling of other hazards such as wave and storm surge or rain fall should be given particular attention in following studies. Similarly, a closer look at the situation in the North Atlantic is required given the concentration of risk exposed to transitioning system in the North East of the United States.

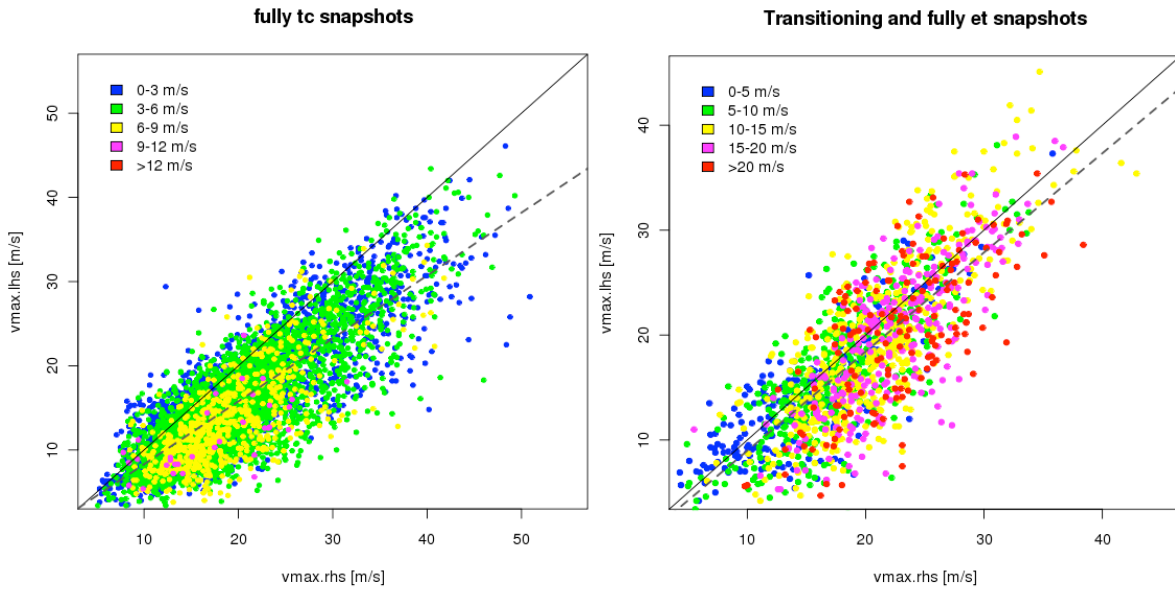


**Figure 2. Maximum 10 m wind speed (at least 100 km) to the left of the track ( $V_{max.lhs}$ ; y-axis) as a function of the maximum to the right of the track ( $V_{max.rhs}$ ; x-axis) for both (a) fully tropical cases and (b) transitioning / fully extratropical cases. Colour bins indicate the storm translational speed in m s<sup>-1</sup>. The 1:1 (solid) and linear regression (dashed) lines are shown.**

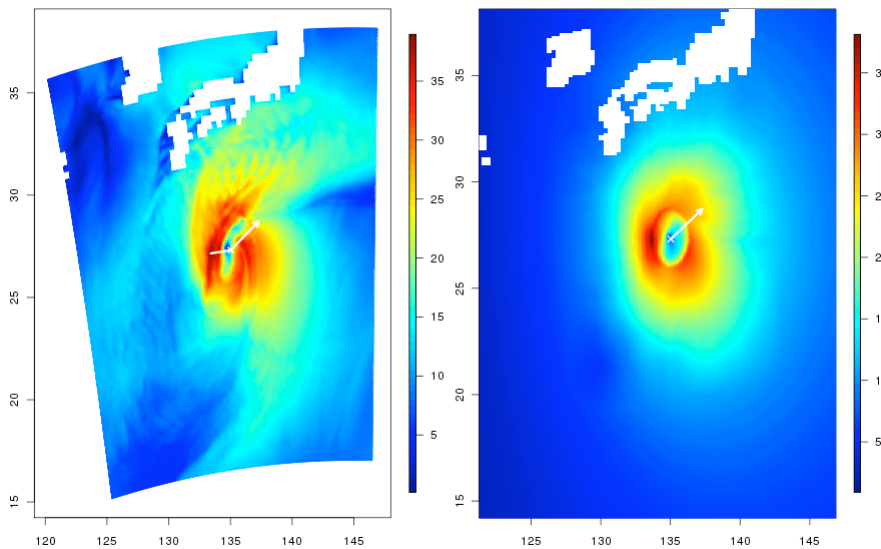


**Figure 3. 10 m wind field simulation for typhoon Rammasun from WRF (left) and the parametric transitioning model (right) at 0600 on the 12<sup>th</sup> May 2008**

### 4.3.3 Operational challenges of ET designation in West Pacific

#### 4.3.3.1 Application and improvement to the objective Cyclone Phase Space method

For a long time, Chinese forecasters judged ET events by satellite images and weather charts at various vertical levels. When colder, drier midlatitude air is entrained into the typhoon centre, operational forecasters will record it as having undergone ET. The frequency of ET classification in current operations has been generally limited to forecaster experience. Under this consideration, the CMA meteorologists consult the CMA/STI Best Track dataset, JMA Best Track dataset and compared with the objective ET CPS method (Hart 2003). A summary of that work is shown in Figure 4

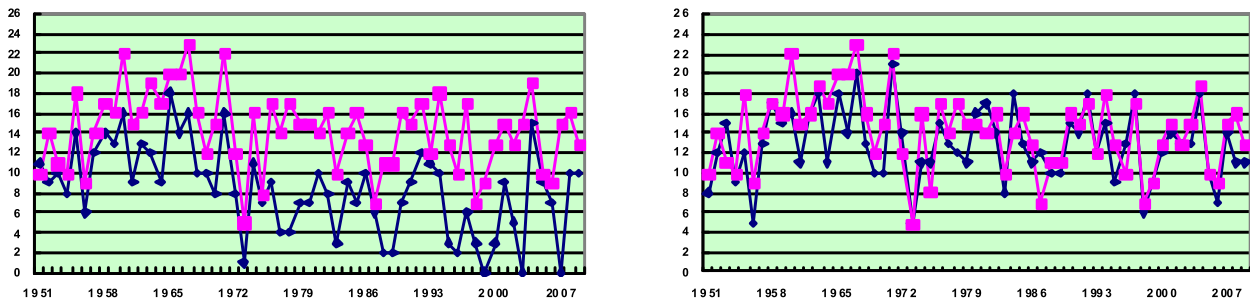


Figure 4. Number of TCs undergoing ET from 1951-2010. Left: STI/CMA and Right: JMA. Dark blue shows the BT and magenta indicates the number of ET events as determined using the CPS method.

Comparing the CPS count with the CMA BT count shows an obvious difference in judging whether ET has occurred. Also there were large differences between the timing of ET – as much as 4 days. There is much better agreement between the JMA-based and the CPS-based ET in the Japan region farther north.

One of the key explanations for these differences seems to be related to the fact that the CPS method is mainly based on thermal structure and not dynamical structure. It is well known that typhoons, especially in the China mainland and South China sea, are affected by complex topography and a southwesterly low-level jet related to the monsoon. Typhoons in the monsoonal zone and traversing complex geography (with varying terrain and land use) will always show some ET-like characters (e.g. asymmetric thermal wind structure) defined in CPS even while it is still a tropical cyclone because cooler air may not necessarily penetrate the typhoon core. In recent years the STI has made improvements on their ET designation classification by augmenting the traditional CPS method with dynamical components such as vertical tilt of the storm core and wind shear magnitude between the 900 and 600 hPa levels.

#### 4.3.3.2 Future challenges and research focus

Through the work of researchers and forecasters in recent years, but challenges remain. One of the most urgent problems in typhoon forecast is how to detect the onset of an ET event and distinguish it from decaying typhoons earlier and more accurately during the forecast evolution. Another challenge in the operational forecasting of ET is diagnosing extreme low-level wind/wind shear which can result in severe wind storms, especially over elevated terrain. These particular operational challenges are aspects in which to focus research and observations.

#### 4.3.4 Structure change metrics and relevance to damage

New metrics for assessing the potential for damage from a TC are likely to become more useful to governments and industries trying to assess monetary risks, when examined in the context of demographic, social and construction parameters. Better resolution of *wind fields* is becoming available to allow researchers and forecasters to better understand the impacts on populations. metrics which include some integration over an area of winds above threshold (or duration of wind speeds above a threshold over a location) are better suited to assessing impacts than 'snapshot' or 1-dimensional measurements of wind speed.

Power Dissipation Index, Cyclone Damage Potential, IKE and TIKE are potentially more useful in their scope to describe the potential for damage than the more traditional wind classification schemes or standard metrics such as maximum sustained wind speed. A cursory analysis of selected landfalling US hurricanes reveals a better relationship between Integrated Kinetic Energy (Powell and Reinhold 2007) and economic damage (Pielke et al, 2008, and Murnane & Elsner 2012), Figure 5, than simply maximum wind speed, Figure 6.

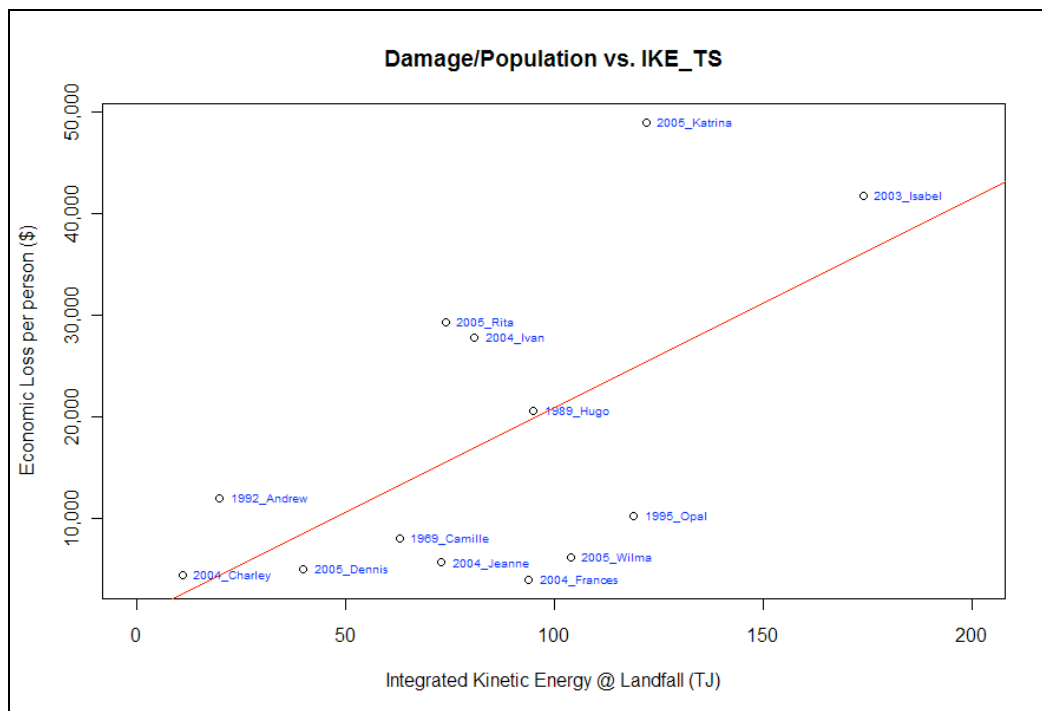
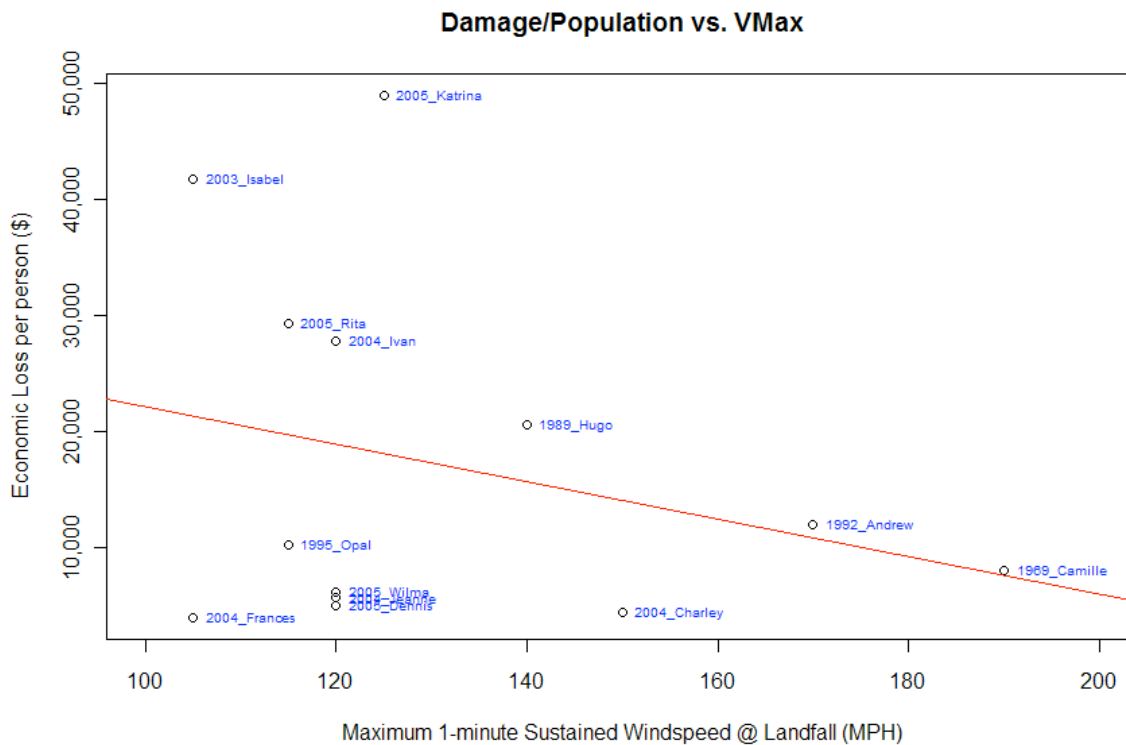


Figure 5. Scatterplot and Linear regression of Integrated Kinetic Energy within the tropical storm wind radius (Powell and Reinhold, 2007), vs. Economic Damage per unit Population (from Murnane and Elsner 2012) Linear regression function is  $y = 206.15x + 289.78$ , with  $R^2 = 0.3581$



**Figure 6. Scatterplot and Linear regression of maximum sustained winds at landfall (Powell and Reinhold, 2007), vs. Economic Damage per unit Population (from Murnane and Elsner 2012) Linear regression function is  $y = -160.37x + 38167$ , with  $R^2 = 0.0725$**

This approach of analyzing the relationship between wind field structure and populations & property at risk reveals a need to more formally include such derived parameters in standardized datasets of tropical cyclone activity. Indeed the simple examination presented here is by no means complete, and these preliminary results would benefit from a more robust sample size. At the very least, this approach motivates the development of larger sets of data to augment the existing wind parameters in the Best Track databases. Some relevant work has been sponsored by the Risk Prediction Initiative follows this motivation.

#### 4.3.5 The effect of island terrain on structure

Yang et al. (2011a) investigated the landfalling characteristics of Typhoon Nari (2001) as it moves across Taiwan Island by performing a series of cloud-resolving simulations of Typhoon Nari (2001) with and without the Island's topography. Various kinematic and precipitation features prior to and after landfall were examined with a focus on the dynamic effects of Taiwan's Island's high topography upon the generation of Nari's asymmetric structures. It was found that tangential winds weaken, whereas the low-level inflows and midlevel outflows increased after landfall due to the increased friction and terrain blocking. The eyewall updrafts exhibited more cellular structures and tended to tilt more outward with height over the high topography of the Island of Taiwan. The radii of the maximum winds and the eyewall updrafts contracted further after landfall, with more pronounced contraction occurring in the portion of the eyewall where more terrain retardation and blocking were present. In particular, the high topography of the Island of Taiwan allowed the elevated low equivalent potential temperature air over the rugged terrain to intrude into the inner-core region, causing the breakdown of the eyewall (Figure 7).

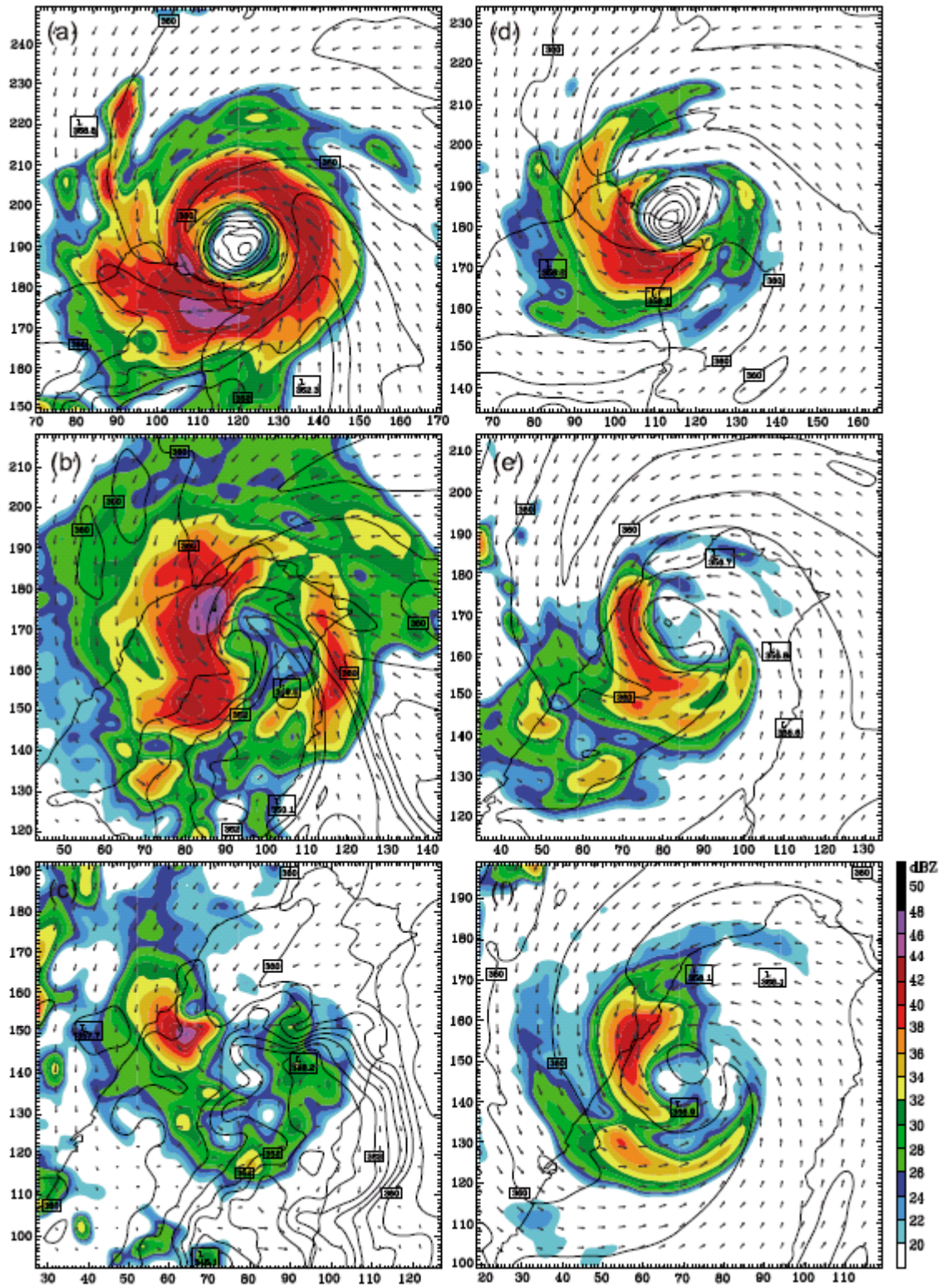


Figure 7. Horizontal distribution of the near-surface ( $s = 0.996$ ) equivalent potential temperature and radar reflectivity (coloured, dBZ), superimposed with the surface flow vectors, from (a, d)  $t = 20$  h, (b, e)  $t = 25$  h, and (c, f)  $t = 30$  h of full-terrain run (Figures 7a, 7b, and 7c) and no-terrain run (Figures 7d, 7e, and 7f)

#### 4.3.6 DA for NWP and improved structure change forecasting

Model forecast uncertainty for TC's depends on a number of factors, including present atmospheric conditions, past and present observations, errors in the forecast model, and assumptions made by the data assimilation system. Ensembles provide a probabilistic estimate of the future model state that is consistent with the underlying system dynamics and observation uncertainty from past data assimilation cycles (Epstein 1969). These statistics, however, are often sensitive to sampling bias, owing to the small ensemble size relative to the state dimension and unresolved errors in the forecast model and observing system. Poterjoy et al. (2014) demonstrate how ensemble error statistics used during data assimilation affect the accuracy of TC structure prediction in models. Using a range of ensemble sizes and various degrees of covariance inflation, this study investigated the effects of sampling bias on the prediction of Hurricane Katrina (2005); experiments focused primarily on EnKF analyses generated by assimilating inner-core airborne radar observations (Weng and Zhang 2011). In the vicinity of observations, 60 members appear to be sufficient for capturing many of the important features of the tropical cyclone inner core in the EnKF analyses. Nevertheless, sampling differences between numerical experiments---even for ensembles larger than 60---produce variations in the outer-core pressure and wind fields that persist for three or more days in simulations.

The impacts of observation coverage and data assimilation strategy are investigated further in Poterjoy and Zhang (2014a,b) using Hurricane Karl (2010) as a case study. Karl was targeted by the Pre-Depression Investigation of Cloud Systems in the Tropics (PREDICT) and the Genesis and Rapid Intensification Processes (GRIP) field campaigns, which provided several days of in-situ measurements before and after genesis. Poterjoy and Zhang (2014a) show large differences in the meso- $\alpha$  scale vorticity, temperature, and moisture fields in EnKF analyses that include PREDICT observations in addition to routinely collected data in cycling data assimilation experiments. These factors yield a 24-h increase in lead time for predicting the genesis and rapid intensification of Karl, compared to a control experiment that excludes the field observations. In a follow-up study, Poterjoy and Zhang (2014b) apply a coupled ensemble-4DVar (E4DVar) data assimilation system to make better use of the dense dataset provided for Karl. This system alleviates some of the issues discussed in Poterjoy et al. (2014) by: 1) using a mix of ensemble and climatological information to estimate forecast error covariance, thus decreasing the impact of sampling bias found in pure ensemble systems; and 2) fitting the analysis state to observations through a time window, which increases the amount of data that can be assimilated during a given assimilation cycle. Deterministic track and intensity forecasts for Karl, initialized every six hours, are plotted in Figure 8, showing large improvements in the timing of genesis and rapid intensification when E4DVar is compared to EnKF and 4DVar methods. Analyses generated during tropical storm and hurricane stages of Karl's development illustrate some of the benefits of using a hybrid E4DVar data assimilation technique. For example, Figure 9 compares EnKF, 4DVar and E4DVar deterministic forecasts from the 18 UTC 14 September cycle. This figure shows the 18-h evolution of 950-hPa positive relative vorticity ( $\zeta$ ) and 950-500-hPa column relative humidity (CRH) in a 450 x 450 km<sup>2</sup> box around the storm centre. The storm in each analysis has an intensity greater than or equal to a tropical depression, however, the E4DVar analysis is more representative of a tropical cyclone than the EnKF and 4DVar cases at this time; e.g., the vortex maintains an annular ring of positive  $\zeta$  around a relatively dry centre. Likewise, E4DVar provides the only analysis that intensifies the low-level vortex immediately after initialization.

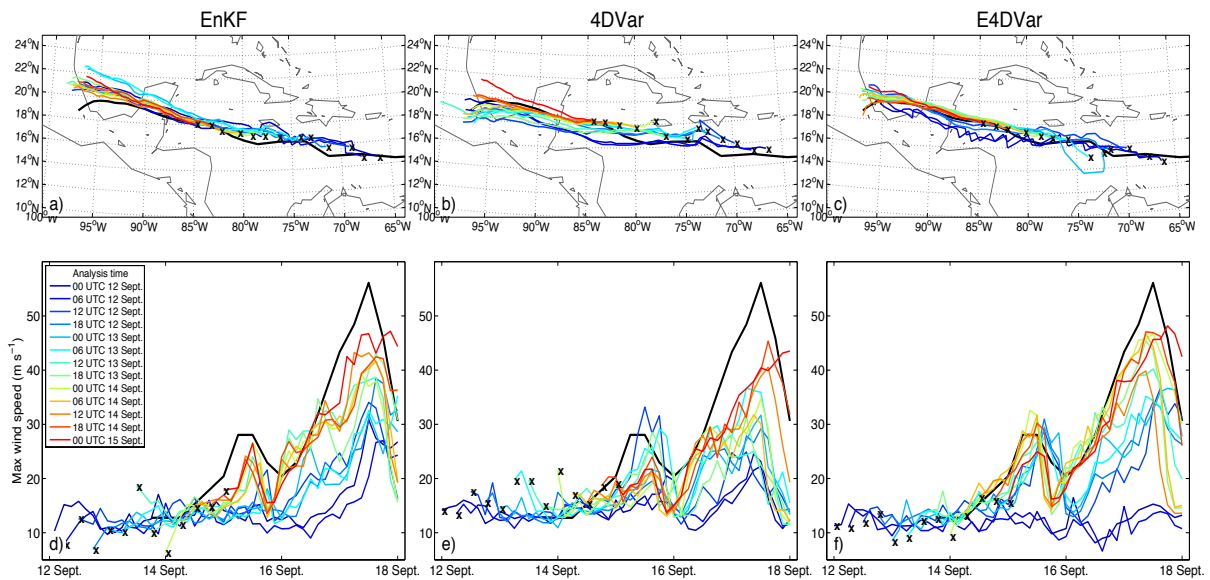


Figure 8. Deterministic (top row) track and (bottom row) intensity forecasts from the (first column) EnKF, (second column) 4DVar and (third column) E4DVar experiments. Forecasts are coloured according to initialization time and NHC best-track data is plotted in black

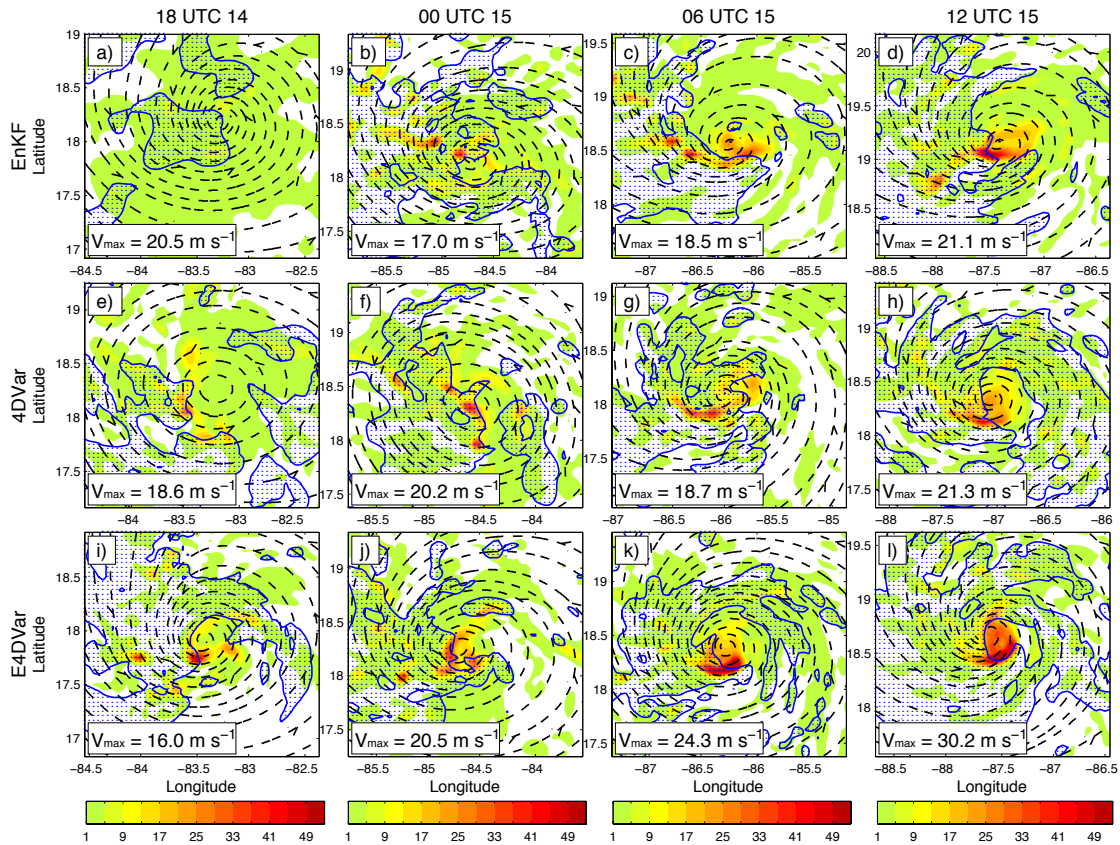


Figure 9. 950-hPa relative vorticity (shaded every  $4 \times 10^{-4} \text{ s}^{-1}$ ), 950-500-hPa CRH values greater than 90% (blue contours), and filtered ( $L > 150 \text{ km}$ ) 950-hPa storm-relative streamlines (dashed black contours) are plotted every 6 h to 12 UTC 15 Sept from forecasts initialized from (top row) EnKF, (middle row) 4DVar, and (bottom row) E4DVar analyses on 18 UTC 14 September

#### 4.3.7 Model initialization of TC structure and intensity – CHC’s perspective

When TCs are not being monitored by aircraft, NWP will often initialize the storm too-weak which has a great impact on the storm’s wind field as well. This deficiency is exacerbated for small, intense storms where the initial central pressure can be up to 50 hPa too high. A storm that is poorly initialized in the model will understandably lead to a poor forecast of both absolute intensity and structure evolution. The model will often intensify the storm vortex from its initial state when the storm may in fact be expected to enter a weakening phase. Forecast production which utilizes output from the model is immediately compromised by the poor initialization, and thus alternative methods such as parametric surface wind and pressure field constructs are necessary. An example of poor initialization in the Canadian Meteorological Service weather model for Hurricane Kyle is exemplified in Figure. 10. The 48-hour forecast verified much better than the 00-hour forecast valid at the same time. Very similar behavior with the model output was observed during the 2011 hurricane season when compact Hurricane Ophelia was being initialized about 40-hPa too weak. The CHC informed its supporting forecast centres that alternative means for objective guidance were required.

Even when model initialization of intensity (e.g. central pressure) is generally good, there remains a need for the operational forecast centre to be able to prescribe the structure (vortex) along an alternative trajectory (the official track) based on the forecaster’s assimilation of all available information, numerical guidance and experience. This requires a simplified wind radii structure or some form of vortex relocation/blending that is prescribed by the forecaster at discrete time intervals and by specified wind thresholds by quadrant around the storm. The ability to do this to pilot wave and storm surge models is paramount in delivering a consistent product.

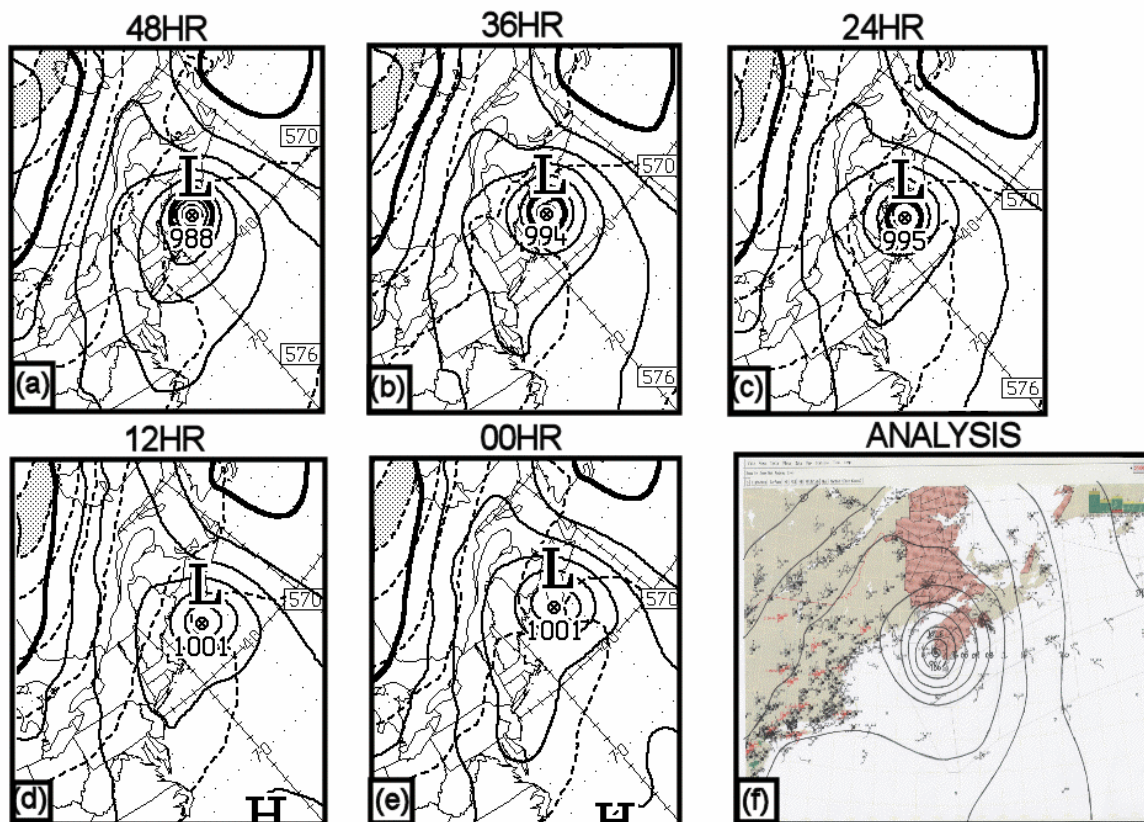


Figure 10. Sea level pressure and 1000-500 mb thickness fields from the GEM REG model for various forecast lead times during Hurricane Kyle, all valid for 00 UTC September 29<sup>th</sup>, 2008. The verifying (analyzed) pressure pattern is shown in panel f.

### 4.3.8 Concentric eyewall cycles and structure

Because of the important roles of double eyewalls in determining hurricane intensity changes, the quasi-balanced framework is used to understand how the development of an outer eyewall could affect hurricane inner-core dynamics during the eyewall replacement period. By treating the outer and inner eyewalls as two idealized rings of PV anomalies, three PV-omega inversions are performed to estimate the quasi-balanced secondary circulations induced by an inner eyewall (Figure 11a), an outer eyewall (Figure 11b), and double eyewalls (Figure 11c), respectively. Results show that the development of an outer eyewall (or spiral rainbands) is inimical to the inner eyewall in several ways, e.g., by (a) adding an anticyclonic flow inside to offset the cyclonic rotation of the inner eyewall, (b) enhancing a ring of a lower pressure zone underneath to broaden the inner-core lower pressure region, (c) inducing an inward (outward) radial flow outside (inside) in the PBL (upper-level) to block the energy supply to (outflow of) the inner eyewall, and (d) generating subsidence between the two eyewalls to suppress the development of deep convection in the inner eyewall. Part of these results supports the hypotheses of Black and Willoughby (1992) and Wang (2009) that the outer eyewall not only acts to reduce the lower-level convergence for maintaining deep convection in the inner eyewall but also induces subsidence over the regions occupied by the inner eyewall.

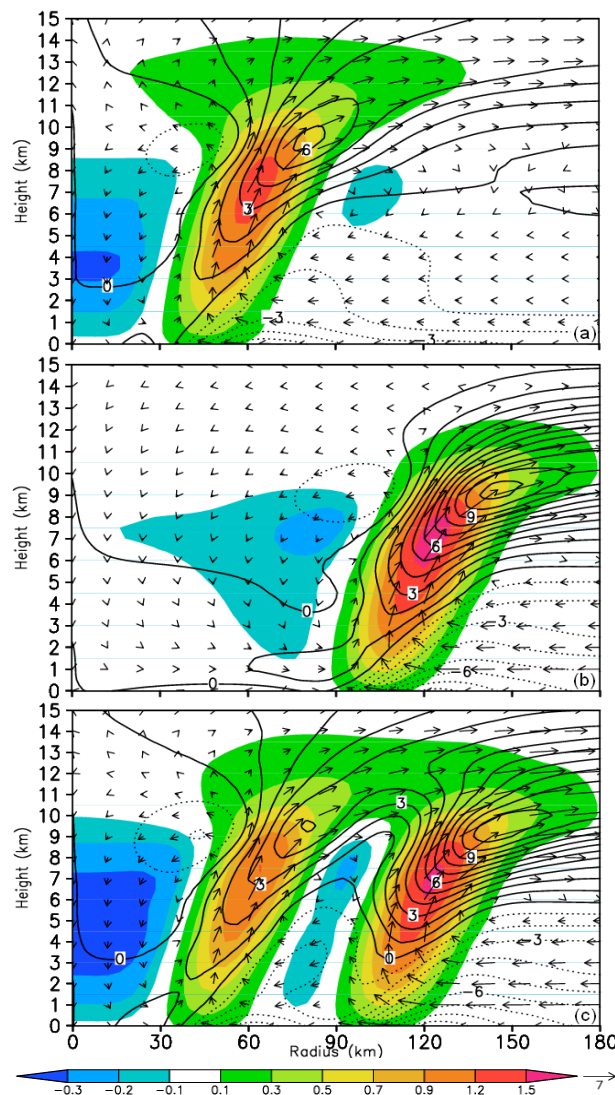


Figure 11. Radius-height cross sections of the quasi-balanced vertical motion (shaded,  $\text{m s}^{-1}$ ) and radial flows (contoured at intervals of  $0.5 \text{ m s}^{-1}$ ), superposed with the resultant in-plane flow vectors, associated with diabatic heating in (a) the inner eyewall; (b) the outer eyewall; and (c) the double eyewalls

#### 4.3.9 Structure representation in NWP and downstream effects

Hurricanes undergoing extratropical transition may strongly impact the midlatitude wave train by amplifying or even triggering Rossby wave trains. This is often accompanied by a reduction in predictability over Europe. One recent example was Hurricane Nadine in 2012, which made medium range forecasts in Europe nearly impossible (pers. Comm. Ansgar Engel, Forecaster at DWD, Pantillon et al., 2014).

Another prominent case was the ET of Hurricane Hanna (2008), which strongly modified the midlatitude wave train. A PV Streamer formed over Europe and eventually caused the formation of a cut-off low over the Mediterranean (Grams et al. 2011). The ET of Hurricane Hanna was also accompanied by a decrease in predictability in downstream regions like Germany. Although the larger scale pattern was not that uncertain, the synoptic situation in Germany, especially for precipitation, was hard to predict (pers. Comm. Ansgar Engel, Forecaster at DWD).

Grams et al. (2011) identified the crucial role of warm-conveyor belt like cross-isentropic airflows that extended from Hanna to the midlatitude jet. Air parcels from the inner core and the eastern sector of Hanna rose to very high levels and proceeded anticyclonically eastward along the midlatitude jet, aiding the strong amplification of the downstream ridge. Additionally, low-PV air was advected into the ridge from the northern part of the transitioning cyclone, expanding the ridge further to the North. In later stages of the ET, those WCB like structures supported the thinning of the downstream trough.

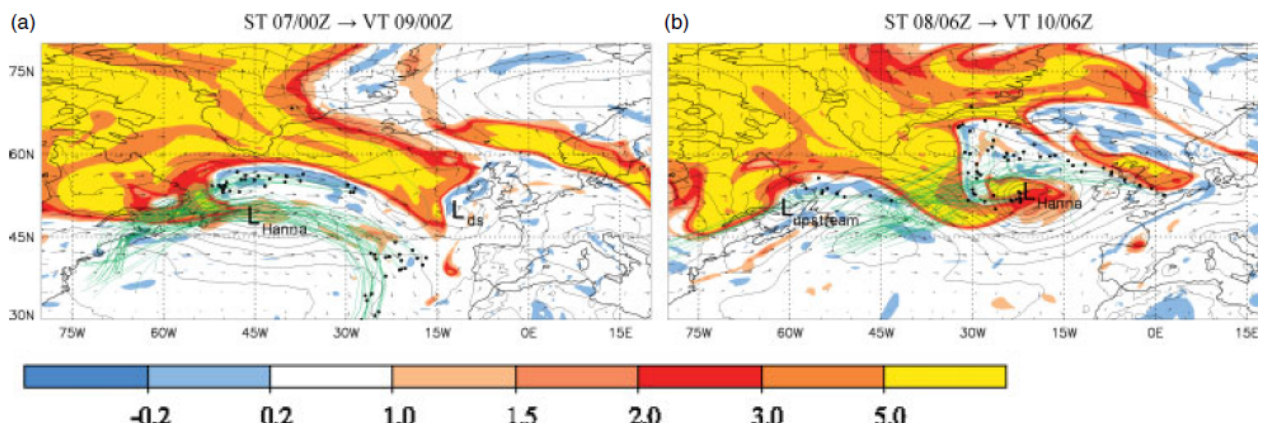


Figure 12. End locations (black dots) of trajectories (green lines), PV (shading) and wind vectors (black) at the 320 K-isentropic level, and pmsl (black contours at 5 hPa intervals). In all two panels, the start times for the trajectory calculation are 48 h prior to the valid times of the meteorological fields and parcel locations, which are (a) 0000 UTC on 9 September 2008, (b) 0600 UTC on 10 September 2008.

The 'L' labels mark the surface centres of cyclones mentioned in the text.

Adaptation of Figure 7 from Grams et al. 2011.

Diabatic processes were also crucial for the reintensification of Hanna as an extratropical cyclone. The remnants of a tropical PV anomaly at lower levels advected (sub-) tropical moist air into the baroclinic zone, where latent heating due to condensational processes led to PV production along the baroclinic zone and the formation of a bent-back warm front. The remnants of the tropical PV were advected southeastward and formed a weak cold front, while the newly generated PV became the new centre of the cyclone. The study of Grams et al. (2011) emphasizes the importance of a correct representation of moist processes during the ET event to correctly predict the structural changes during ET. On the one hand, those processes impact the transformation from a tropical to an extratropical system. On the other hand they play an important role in the modification of the midlatitude wave train.

#### **4.3.10 Use of Aircraft Observations to Diagnose and Predict Structure Change**

##### **4.3.10.1 Research Findings from Vortex Data Messages**

Through support from the Risk Prediction Initiative (RPI2.0), the Vortex Data Message Dataset (VDM+) has been completed and will soon be released to the public. This dataset comprises over 5600 VDMs taken in Atlantic, Eastern Pacific, and Central Pacific TCs from 1989 – 2012. Thus far, the VDM+ dataset has been used to investigate the structure and intensity changes that occur during eye formation (Vigh 2010; Vigh et al 2012) and to explore the potential usefulness of these data to predict rapid intensity change (Vigh and Rozoff 2012). Vigh (2012) analyzed the statistics of Atlantic TC eye formations over that period and found that TCs tend to form an eye detectable by aircraft (and presumably microwave imagery) at a central pressure of  $991 \pm 9$  hPa, at an analyzed Best-Track intensity of  $30 \pm 8$  m s<sup>-1</sup> ( $58 \pm 16$  kt), and with a radius of maximum wind (RMW, at flight level) of  $34 \pm 35$  km (these statistics provide the median value at eye formation along with the Inter-Quartile Range). In 83% of these cases, the aircraft observed the eye prior to becoming detectable by IR satellite imagery. Once genesis occurs, TCs tend to form an eye within 48-h of reaching tropical storm strength. A key finding is that the wind maxima associated with the developing TC inner core tend to contract significantly in the 24-h prior to the formation of the eye. Storms are often intensifying rapidly at the time of eye formation, so eye formation often serves as a structural marker to indicate that consolidation of the RMW has probably taken place and that rapid intensification is likely occurring. Figure 13 shows a visualization of several of the VDM intensity and structure parameters for the life of Hurricane Isidore (2002). This storm is a prototypical example of a class of TCs that tend to experience dramatic RMW contraction prior to eye formation. Once the eye has formed, the RMW tends to continue slowly contract or contraction ceases altogether.

# ISIDORE (AL102002)

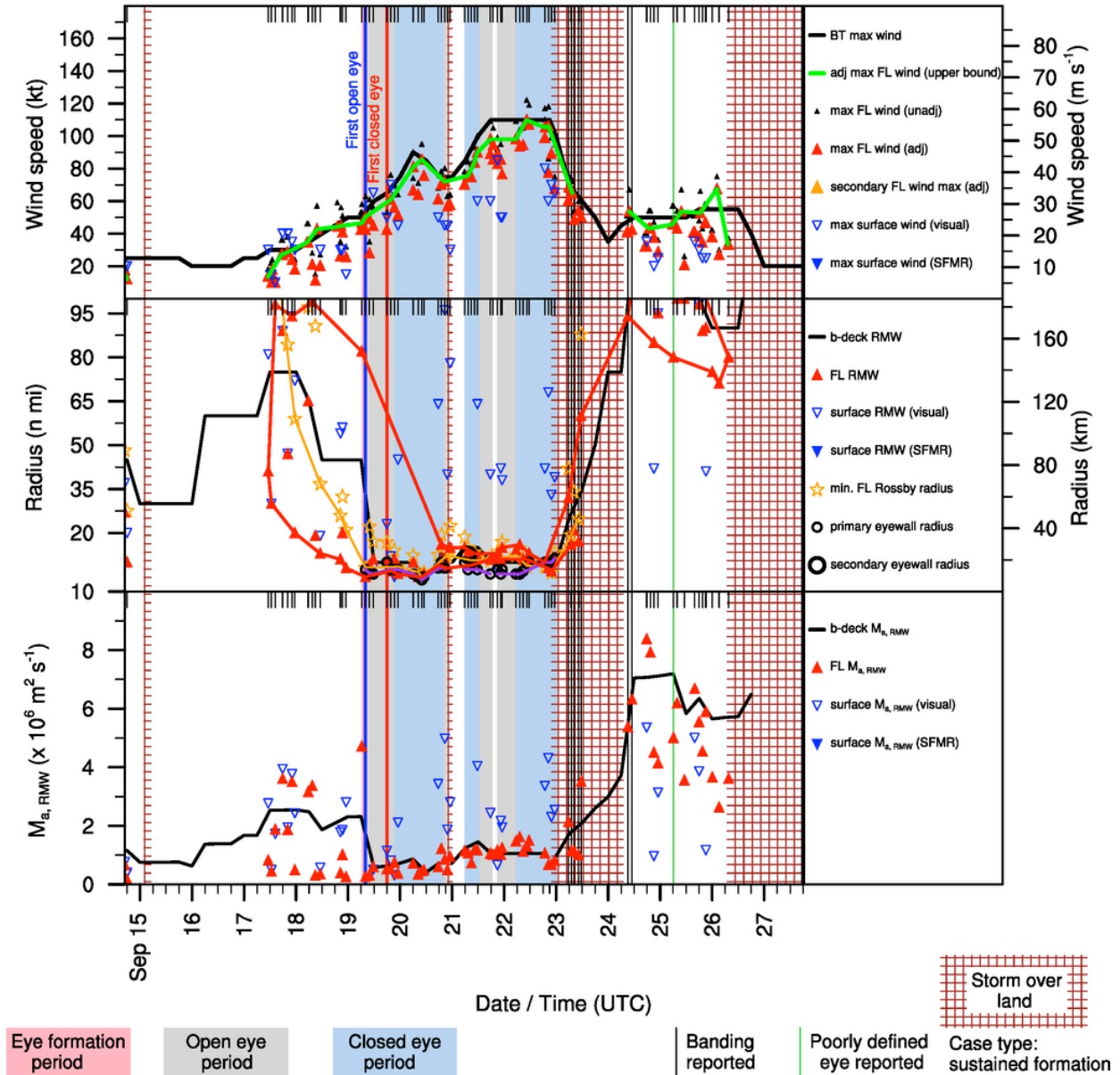


Figure 13. Example of visualization of structural parameters from VDMs over the lifecycle of Hurricane Isidore (2002). Top panel shows the following intensity parameters: Best Track intensity (black curve), flight level wind speed maxima reduced to a surface equivalent (red triangles), and the upper bound of the surface equivalent wind speeds (green curve). Middle panel shows the following size parameters: RMW from the ATCF b-decks (black line), radius of maximum winds at flight level (red triangles), and eye radius (circles).

More recently, the VDM data have been analyzed to determine the RMW changes that occur as the storm intensifies past various intensity thresholds. By only taking the RMW values at the point in which a storm *first* surpasses each intensity threshold, one can glean the typical RMW evolution during the primary intensification phase of the TC. Figure 14 shows the result of this analysis. As suggested by the previous research on eye formation, TCs tend to contract most rapidly in the same range of intensities in which eye formation tends to occur, contracting from a median RMW of 80 km at 35 kt, to approximately 45 km by 55 kt. For intensities of 65 kt and

above, the rate of RMW contraction slows considerably. This suggests that eye formation stabilizes the storm to further contraction.

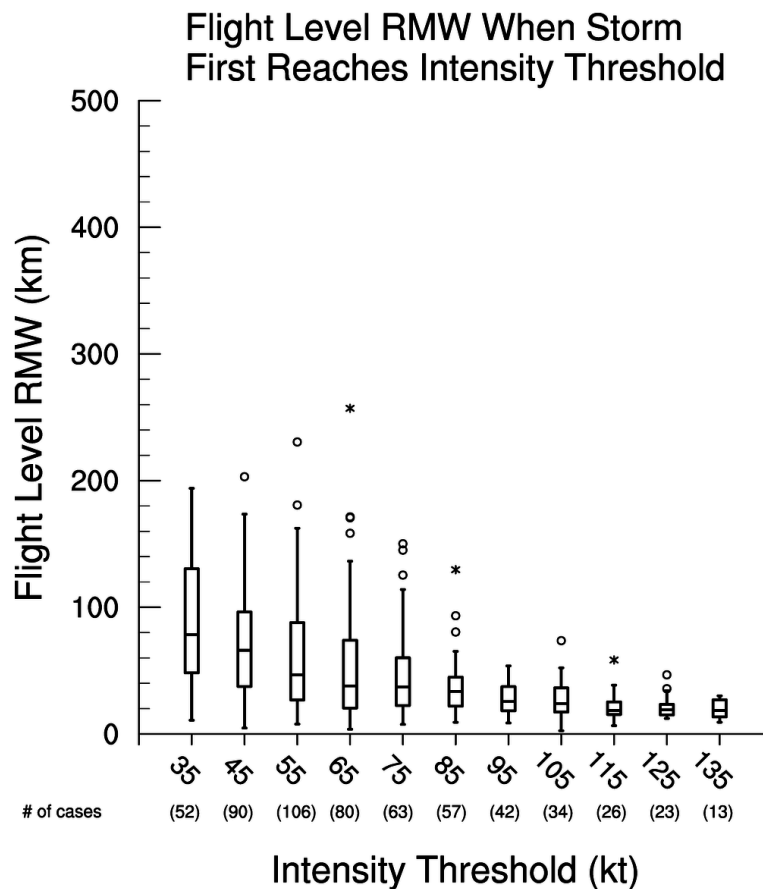


Figure 14. Box-and-whisker plot showing the observed flight level RMW at the time when each storm *first* achieves the given intensity threshold. This plot was constructed by binning the RMW values only at the time point when the interpolated Best-Track intensity of the storm first reaches the given threshold. The binning is as follows: the '35' bin contains all cases where the intensity is less than 35 kt, the '45 kt' bin contains all the cases where the intensity is  $\geq 35$  kt and  $> 45$  kt, etc.

#### 4.3.10.2 An Extended Flight Level Dataset

Through support from RPI2.0, all available flight level data from 1999 – 2013 have now been standardized, processed, parsed into radial legs, and binned into a standard radial grid at a 100-m grid increment. Efforts have been undertaken to ensure that the flight level wind speeds are of high quality. Additionally, an algorithm has been developed to filter out (as much as possible) inaccurate retrievals of surface wind speed from the Stepped Frequency Microwave Radiometer (SFMR). Such artifacts can occur when the instrument flies over land, very shallow water ( $< 5$  m depth), or when the plane is rolling or turning sharply. Figure 15 shows an example of the radial leg data parsed from a flight in Supertyphoon Megi (2010), which had the highest measured wind speeds in the entire data set. The resulting *Extended Flight Level Dataset* (FLIGHT+) seeks to mimic the characteristics of the Willoughby-Rahn flight level dataset to provide research-grade wind speed data in both earth-relative and storm-relative reference frames. The wind information is also decomposed into radial and tangential components. Output is provided in a modern Network Common Data (NetCDF) file format. The FLIGHT+ dataset will be released to the public in 2015.

#### 4.3.10.3 Using Flight Level Data for Advanced Verification and Guidance-on-Guidance

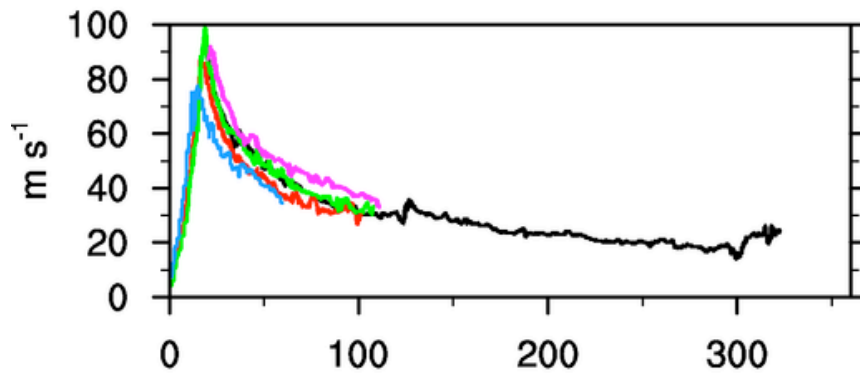
An important part of the forecast process is for the forecaster to assess how well each numerical weather prediction (NWP) model has analyzed the tropical cyclone (TC). Often, poor model analyses of storm structure lead to subpar model predictions of intensity and structure. If the “goodness” of the model’s storm structure can be accurately assessed by the forecaster (or an objective technique), it should be possible to “handicap” the model predictions to discount models with a poor analysis and place greater weight on the models that represented the storm well. Currently, forecasters assess the goodness of model analyses (and near-term forecasts) by visually comparing aircraft or satellite data with the model fields either at select points, or using observational analyses of the data. An operational capability does not yet exist to *directly* compare the model’s simulated storm structure to the observations in a storm-centred framework. To do so fairly, one must account for the factors of the storm motion, the pressure height of the observing platform, and model-dependent resolution. Having such a capability would expedite the analysis and forecast process and provide additional types of information that can then be used to provide “guidance on guidance”, thereby improving intensity and structure forecasts.

With the support of the Development Testbed Center Visitor Program (DTCVP), Dr. Vigh has recently developed a module to conduct direct comparisons between the wind and thermal structures of NWP model simulations the flight level and remotely sensed surface observations from reconnaissance aircraft. The *synthetic profiles* technique shows great promise to facilitate these types of direct observation-to-model comparisons (Vigh et al 2014; Vigh 2014). To construct the synthetic profiles (or in this case, synthetic radial legs), the aircraft observations are first processed extensively to put the data into a frame of reference moving with the storm. The motion of the storm during the observational sampling period is accounted for, resulting in accurate storm-relative wind speeds and radial and tangential wind components. Code has also been automated to objectively identify the “good” radial legs that penetrate the storm centre. Then the model space is sampled by “flying” along trajectories that correspond to the actual radial legs in the real storm, but which have been translated to the centre of the simulated storm. Sampling is accomplished by interpolating horizontally and vertically from the model grid points that lie nearest to each synthetic trajectory point. Each of the synthetic radial legs that result thus has identical storm-relative track and pressure altitude characteristics to the corresponding observed storm-relative radial leg. An appropriate smoothing filter can then be applied to the observed radial profile to allow for a fair comparison with the model. Such synthetic legs can be constructed not just for flight level wind speed, but also for flight level temperature and moisture quantities, extrapolated sea level pressure, and SFMR surface wind speed and rain rate. Synthetic legs can also be constructed and compared for dynamical and thermodynamic diagnostic quantities such as vorticity, inertial stability, and  $\theta_E$ . Code to create synthetic legs has recently been prototyped and run for Hurricane Sandy using HWRF model fields. Figure 15 shows a plan view of the real and synthetic trajectories used to derive synthetic radial legs of the flight level wind speed for a 51-hr forecast from the model cycle initialized at 00Z on 23 October 2012. Figure 16 compares the resulting synthetic radial legs of flight level wind speed for that model time slice with the observed radial legs in the real storm. The plot shows that the model wind structure is fairly close to the observed wind structure on the east side of the storm (longer radial legs), but quite different on the west side (shorter radial legs).

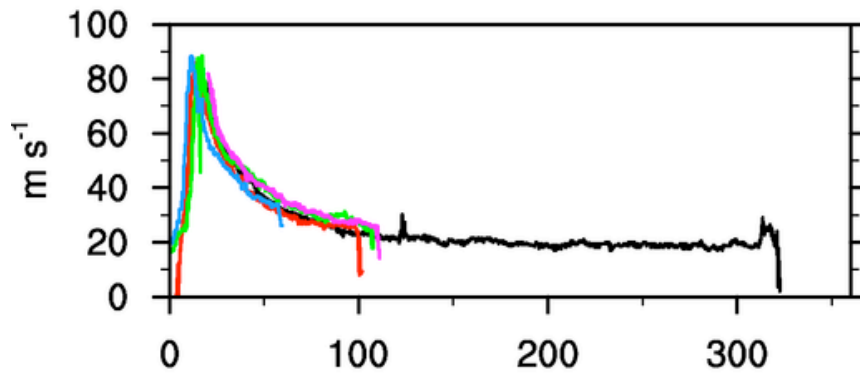
Synthetic profiles offer an intriguing opportunity to improve the prediction of structure change. Statistical techniques can be developed to determine which NWP models are likely to have superior forecasts based on their errors at analysis time and recent model performance. The output of such techniques could provide “guidance-on-guidance” for the forecast metrics of intensity and structure and be used to construct weighted ensembles.

# Megi (2010) FlightID: 20101017U1

Flight Level Wind Speed (earth relative)



SFMR Wind Speed (no QC)



SFMR Wind Speed (QC'd)

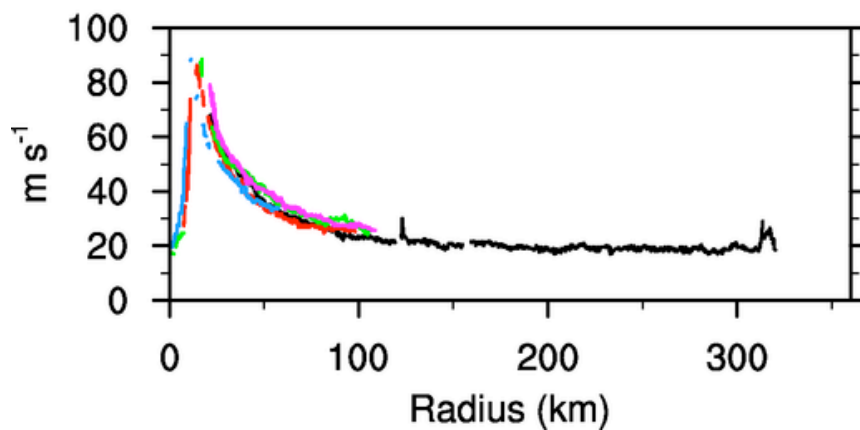


Figure 15. Radial legs for Supertyphoon Megi (2010). Shown are: earth-relative flight level wind speed (top panel), retrieved wind speed from the SFMR instrument prior to quality control measures being applied (middle panel), and SFMR surface wind speed after quality control measures (bottom panel).

# Hurricane Sandy

## HWRF Wind Speed Near Flight Level

Analysis:  
2012102300

Forecast hour:  
051

Valid:  
2012102503

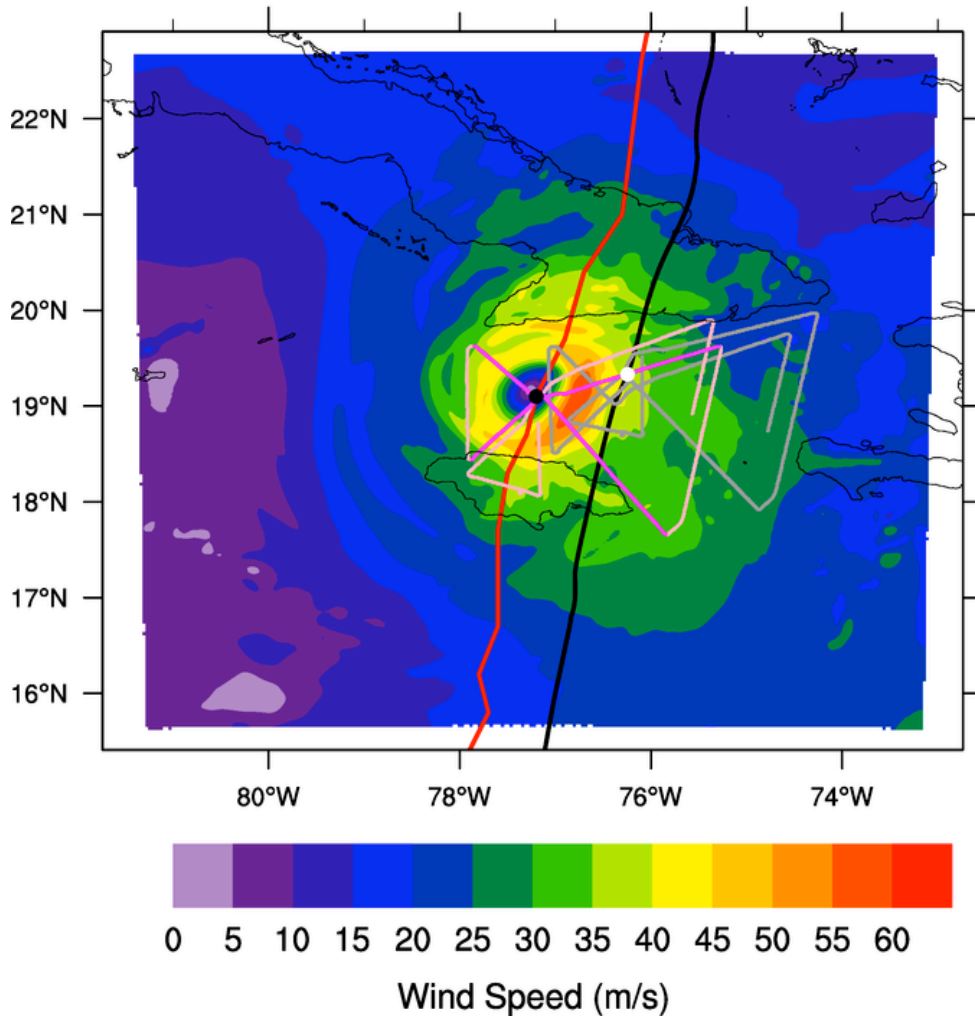


Figure 16. Comparison between the actual flight trajectory in the real Tropical Storm Sandy (grey curves) and the simulated trajectory that has been navigated onto the centre of the HWRf-simulated Sandy (pink curves) for the 51-h forecast from the model cycle initialized at 00Z on 23 October 2012. The portions of the trajectory that correspond to the synthetic radial legs are also shown (magenta curves). For reference, the plot also displays the wind centre track of the actual storm (black curve), the corresponding track of the HWRf-simulated storm (red curve), the position of the real storm at the analysis time (black dot), the position of the simulated storm at the analysis time (red dot), the position of the real storm at the time slice valid time (white dot), and the position of the simulated storm at the time slice valid time (black dot). The model's simulated wind speed is shown (colour contours) at the pressure level nearest that of the average pressure of the first radial leg.

# Hurricane Sandy (2012)

Analysis:  
2012102300

Forecast hour:  
051

Valid:  
2012102503

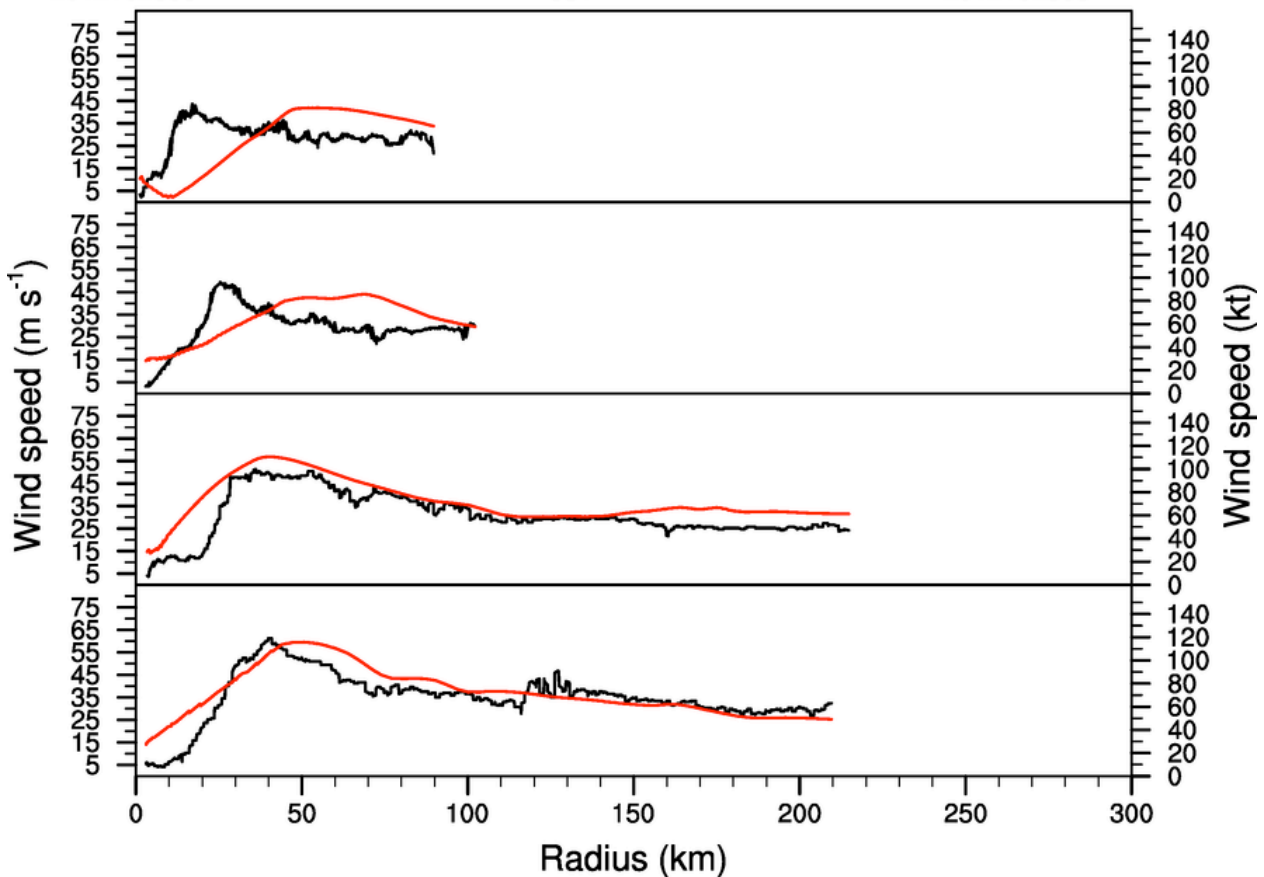


Figure 17. Comparison between the observed radial structure of flight level wind speed in the real storm (black curves) and the synthetically-derived flight level wind speed in the HWRP-simulated storm for each of two radial legs that fell within the match window for the 51-h forecast from the model cycle initialized at 00Z on 23 October 2012

## 4.3.11 Structure prediction in the HWRP system

Here we present a summary of examples of storm structure verification conducted by the EMC HWRP team.

### 4.3.11.1 Forecast verification of the storm size

Figure 18 shows the verification of the mean 34-kt (R34), 50-kt (R50) and 64-kt (R64) radii for the NATL basin for the 2010-2011 hurricane seasons. Here, the R34 at each quadrant is defined as the radius at which the mean tangential wind is equal to 34-kt (and similarly for R50 and R64), and the mean radii are obtained by taking an average of the radii in four different quadrants. Here the operational HWRP run at 9km resolution near the hurricane core (HOPS, blue) is compared against the newly implemented triple nested HWRP model in 2012, operating at 3km resolution near the hurricane core (H212, red).

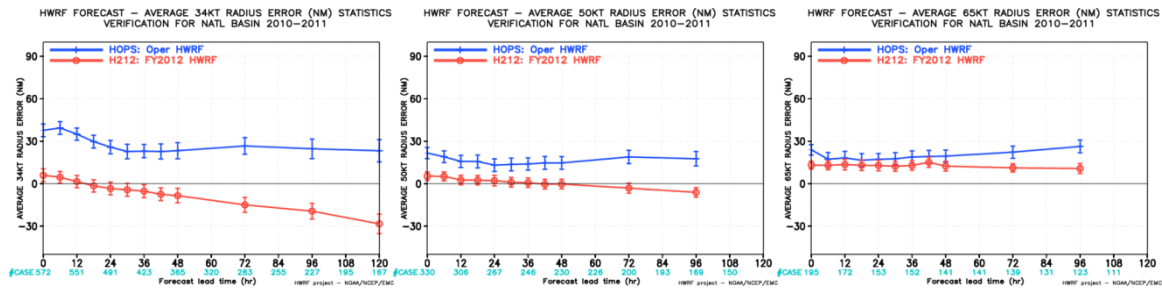


Figure 18. Comparison of the radii verification of the mean 34-kt, 50-kt, and 64-kt radius between the FY2011 operational HWRf (HOPS, blue) and the FY2012 model implementation (H212, red), calculated by using the arithmetic mean of the radii in the SE, SW, NE, and NW quadrants (Tallapragada et al. 2013, MWR)

Except for the R34, the overall reduction in the radii errors by H212 is nearly 80% at all forecast lead times, particularly for R50 and R64. Such a large reduction of the strong wind radii errors indicates that the high-resolution HWRf storm forecasts were able to more realistically capture the inner-core region of the storms. This is expected as storm structure and fine-scale processes are believed to be better resolved with higher resolution. Detailed analysis of these radii errors show that the improvements in the new HWRf configuration could be attributed to more advanced vortex initialization procedure and improved physics, which could help take into account storm structure information at different quadrants more effectively. Such remarkable improvements in the storm structure are observed not only at the initial time but also consistently during entire forecast period as seen in this example.

#### 4.3.11.2 Storm structure forecasts as revealed by the pressure-wind relationship

The relationship between the forecasted PMIN and VMAX is another important measurement for internal consistency of the model dynamics that the simple statistics of VMAX or PMIN errors cannot provide. This is because such pressure-wind relationships (PWR) can characterize a more general internal structure associated with the mass and wind distribution, especially within the inner-core region where the gradient wind balance is well approximated. Figure 19 shows the scatter plot of the model simulated VMAX and PMIN and the corresponding best-fit observed PWR populated from best track data during the entire 2010-2011 hurricane seasons in each basin for both the HOPS (right panels) and H212 (left panels) configurations. One notices that unlike the HOPS configuration in which the model best-fit PWR is substantially different from the observed PWR, the H212 configuration produced a consistent scattering of VMAX and PMIN compared to the observations. The overall HWRf predicted VMAX and PMIN are well centred on the observed error best-fit PWR with  $R^2 \sim 0.8$  for the NATL basin and even higher (0.94) for the EPAC basin (not shown).

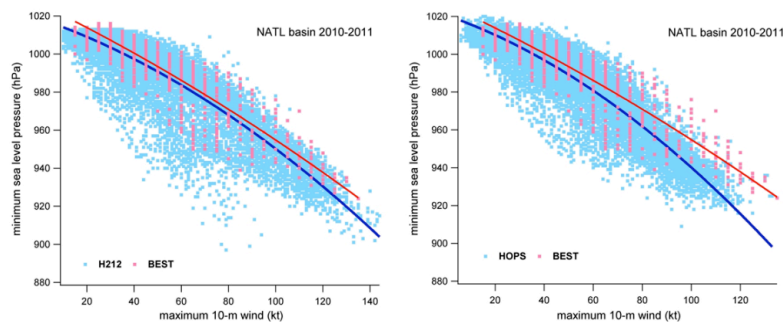


Figure 19. Scatter plots of the VMAX and PMIN from the 2011 operational HWRf version (HOPS, right panel) and the 2012 implementation (H212, left panel) with respect to the best track observation (BEST). Blue dots denote the model forecast values, and red dots denote the observed values. Solid lines are the second-order polynomial best fit.

#### 4.3.11.3 Dynamical constraints related to vortex initialization

Another aspect of the internal dynamical relationships that could be used to evaluate the model performance is the correlation of changes of VMAX and PMIN during the first 6 hours of model integration (termed as initial spin-up/spin-down of model vortex). This correlation indicates how much the model initial vortex is adjusting with the environment during the first 6-h period, which is critical to monitor the performance of the model vortex cycling processes. By cycling the model predicted vortex, we are carrying model consistent TC evolution information to the current cycle, and make small corrections to the 6h predicted vortex either through vortex initialization or data assimilation to improve the vortex structure without completely rebuilding a new vortex. As such, behavior of the storm structure is largely influenced by this initialization processes that provides useful information to the forecasters on storm structure forecast guidance.

Figure 20 shows the stratification of the first 6-h changes of VMAX (black bars) and PMIN (gray bars) with respect to the storm initial intensity for both the HOPS (right panel) and H212 (left panel) configurations. The large initial spin-up/spin-down of the HOPS configuration apparently indicates that the model initial conditions are not well balanced, leading to the rapid short-term intensity changes. For the H212 configuration, it is promising to see that the magnitude of 6-h changes for both VMAX and PMIN is much reduced. In addition, there are no prominent spin-up or spin-down issues for either weak or strong storms. The overall reduction in the initial spin-up/spin-down is a clear demonstration that the model initial vortex is better aligned to its environment in the H212 configuration.

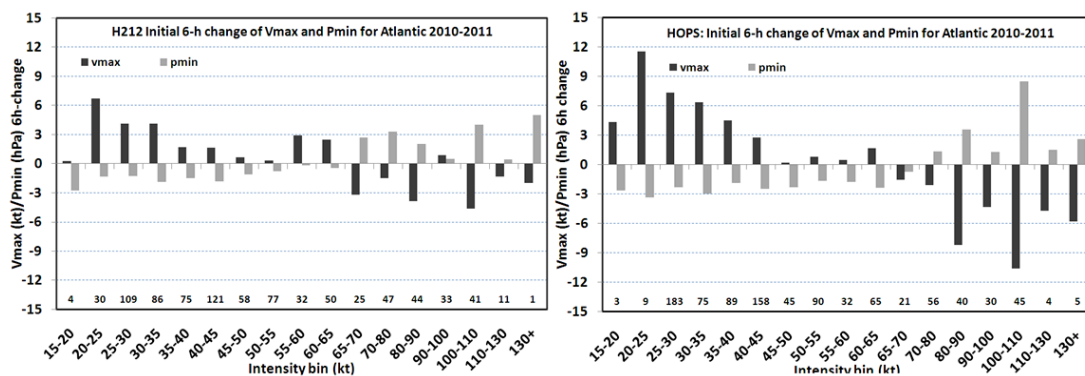
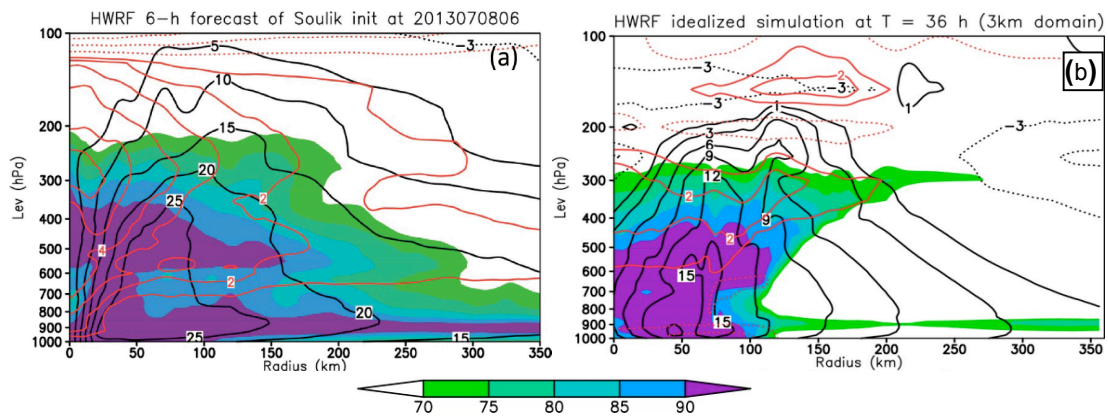


Figure 20. Stratification of the first 6-h change of the maximum 10-m wind (VMAX, black bars, unit kt) and the minimum surface pressure (PMIN, gray bars, unit hPa) of the 2011 operational HWRf model (HOPS, right panel) and the 2012 implementation (H212, left panel)

#### 4.3.11.4 Storm structure evaluation at the onset of Rapid Intensification (RI)

Along with the need to examine the storm size and dynamical constraints for vortex initialization, practical operation of the HWRf model during the last few seasons, particularly the experimental real-time forecasts in the Western North Pacific basin, recently showed that the HWRf model tends to exhibit a consistent structure at the onset of all rapid intensification (RI) events. Examination of real-time HWRf forecasts for Typhoon Soulik just before it started rapidly intensifying on 8<sup>th</sup> July 2013 in the Western Pacific (Figure 21a) showed that the RI onset in the HWRf model appears to be determined by a specific constraint in the dynamical and thermodynamic structure including an upper level warm anomaly of 1-3<sup>0</sup>K, a moist column with relative humidity > 90 % within the storm central region, and sufficient tangential flow (greater than 12 m s<sup>-1</sup>) from low to midlevels (Tallapragada and Kieu, 2014).



**Figure 21 (a) Radius-height cross section of the relative humidity (shaded), the tangential wind (black contours), and potential temperature anomalies with respect to the far-field environment (red contours) in the HWRf forecast for Typhoon Soulik at the onset of RI (Tallapragada and Kieu, 2014). (b) Phase lock conditions in an idealized experiment with HWRf model, showing the vortex structure at the time of RI (Kieu et al. 2014)**

Idealized experiments with different vortex initial vertical structures in different ambient environments confirmed the presence of such equilibrium between model thermodynamics and storm circulation. Analysis of the vortex structure in the idealized experiments at the moment when RI begins (Figure 21b) revealed that this constraint is critical for the RI onset in both dry and moist experiments. No matter how different the vortex structures or favourable the environment conditions are for TCs to grow, the model vortex does not intensify if the above constraint among the tangential flow, the moist structure and the upper level warm core (referred to as phase-lock condition, Kieu et al. 2014) is not established. As soon as such phase-lock occurs, the vortex starts to intensify rapidly.

In another recent study, Chen and Gopalakrishnan (2014) have examined the structural evolution of the Atlantic Hurricane Earl of 2010 during as captured by the operational HWRf model. In this study, the HWRf forecasts are verified against available observations and analyzed to understand the asymmetric rapid intensification of a storm in a sheared environment (Figure 22). The forecast verification showed that the HWRf model well captured Earl's observed evolution of intensity, convection asymmetry, wind field asymmetry, and vortex tilt in the pre-rapid and rapid intensification (RI) stages. The vortex tilt was large at the RI onset and decreased quickly once RI commenced, suggesting that vertical alignment is the result instead of the trigger for RI.

The RI onset was found associated with the development of upper-level warming in the eye centre, which results from upper-level storm-relative flow advecting the subsidence warming in the upshear-left region towards the low-level storm centre, with dominant and persistent convective bursts (CBs) concentrated in the downshear-left quadrant. The temperature budget indicated that horizontal advection played an important role in the development of upper-level warming in the early RI stage with the asymmetric intensification process through cooperative interaction of the convective-scale subsidence, resulting from CBs in favoured regions and the shear induced mesoscale subsidence.

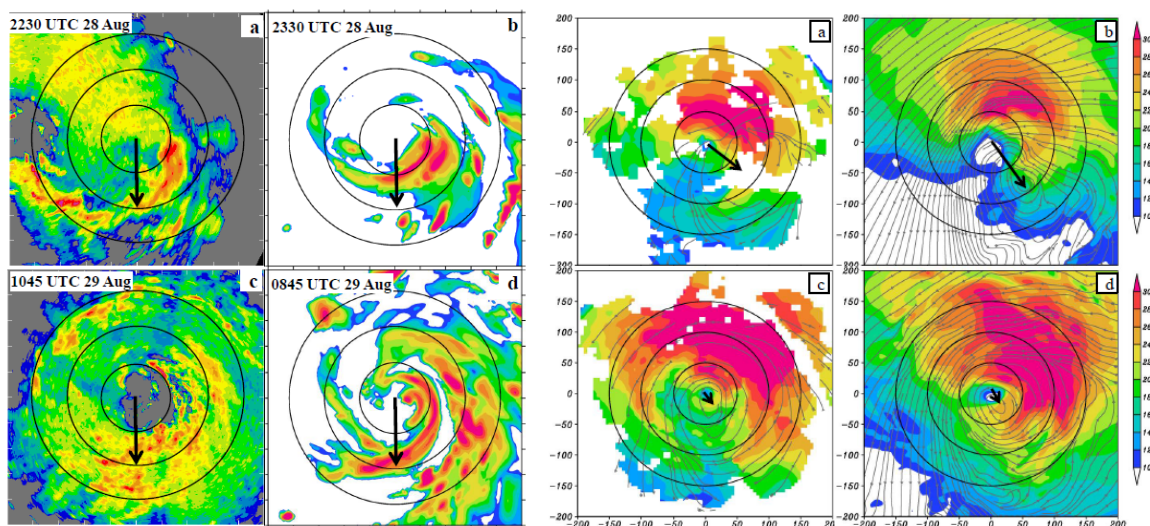


Figure 22. Left Panel: (a) Lower fuselage radar observation of radar reflectivity at 2230 UTC 28 Aug; (b) HWRF forecasted radar reflectivity from the 29.5-h forecast (valid at 2330 UTC 28 Aug); (c) Lower fuselage radar observation of radar reflectivity at 1045 UTC 29 Aug; and (d) HWRF forecasted radar reflectivity from the 62.75-h forecast (valid at 0845 UTC 29 Aug). Right Panel: Wind speed (shading) at 2-km altitude and stream-line (grey lines) at 8-km altitude from (a) composite radar observation in the pre-RI stage; (b) HWRF forecast in the pre-RI stage; (c) composite radar observation in the RI stage; and (d) HWRF forecast in the RI stage. The black circles indicate the 50-km, 100-km, and 150-km radii, and the black arrow indicates the tilt direction.

#### 4.3.11.5 SHIPS diagnostics for structure and structure change information

In addition to the internal model diagnostic tools, the EMC HWRF team has been monitoring the tropical cyclone inner core structure and its environment using various operationally available tools. One of such most frequently use products come from the Statistical Hurricane Intensity Prediction Scheme (SHIPS), developed by DeMaria and co-workers at CIRA. This diagnostic output produces a simple ASCII file with all necessary information for the SHIPS model predictors based on the gridded data input in the GRIB format. The main applications of the SHIPS diagnostics are for the Statistical Prediction of Intensity with a Consensus Ensemble (SPICE) forecasts based on various operational global and regional dynamical models. The derived information from SHIPS diagnostic parameters has recently demonstrated some valuable information about the statistics of the model-predicted large scale variables as well as verification of the synthetic satellite brightness temperatures simulated by the HWRF model compared to Geostationary Operational Environmental Satellite (GOES) imagery.

#### 4.3.12 Model initialization of TC structure and intensity – CHC’s perspective

When TCs are not being monitored by aircraft, NWP will often initialize the storm too-weak which has a great impact on the storm’s wind field as well. This deficiency is exacerbated for small, intense storms where the initial central pressure can be up to 50 hPa too high. A storm that is poorly initialized in the model will understandably lead to a poor forecast of both absolute intensity and structure evolution. The model will often intensify the storm vortex from its initial state when the storm may in fact be expected to enter a weakening phase. Forecast production which utilizes output from the model is immediately compromised by the poor initialization, and thus alternative methods such as parametric surface wind and pressure field constructs are necessary. An example of poor initialization in the Canadian Meteorological Service weather model for Hurricane Kyle is exemplified in Figure 23. The 48-hour forecast verified much better than the 00-hour forecast valid at the same time. Very similar behavior with the model output was observed

during the 2011 hurricane season when compact Hurricane Ophelia was being initialized about 40-hPa too-weak. The CHC informed its supporting forecast centres that alternative means for objective guidance were required.

Even when model initialization of intensity (e.g. central pressure) is generally good, there remains a need for the operational forecast centre to be able to prescribe the structure (vortex) along an alternative trajectory (the official track) based on the forecaster’s assimilation of all available information, numerical guidance and experience. This requires a simplified wind radii structure or some form of vortex relocation/blending that is prescribed by the forecaster at discrete time intervals and by specified wind thresholds by quadrant around the storm. The ability to do this to pilot wave and storm surge models is paramount in delivering a consistent product.

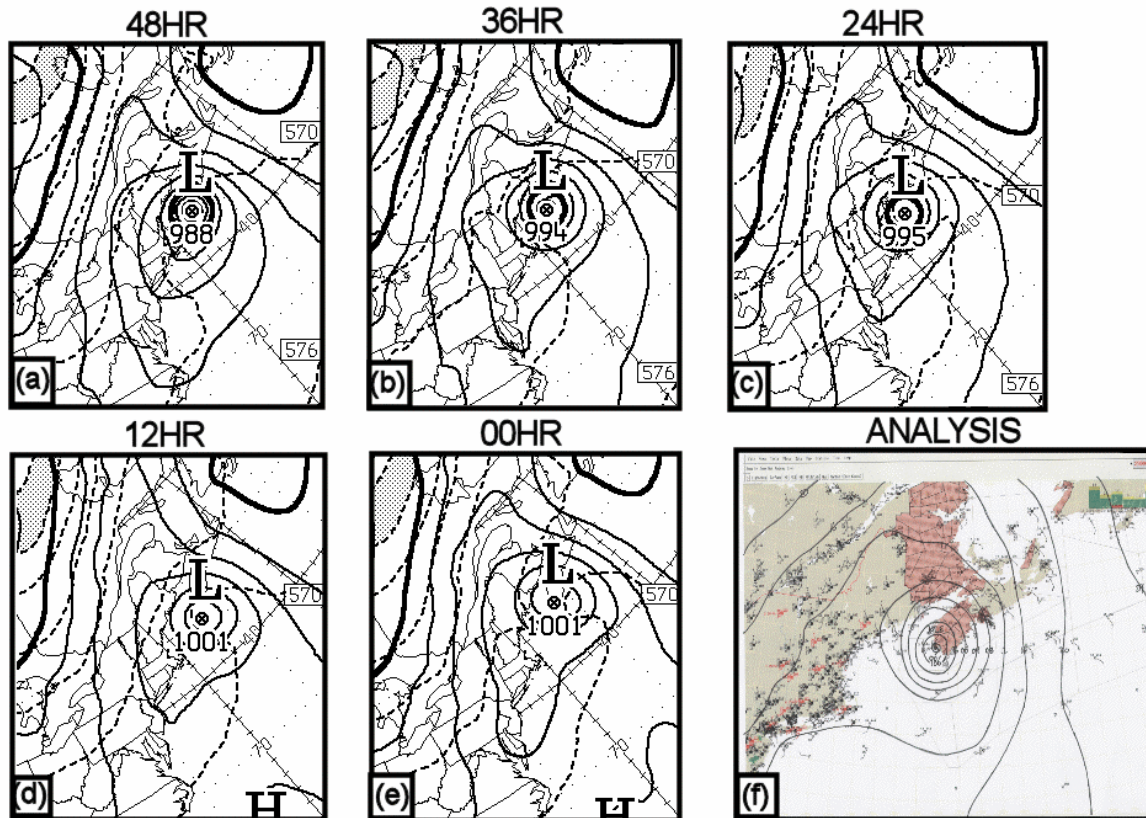


Figure 23. Sea level pressure and 1000-500 mb thickness fields from the GEM REG model for various forecast lead times during Hurricane Kyle, all valid for 00 UTC September 29<sup>th</sup>, 2008.

The verifying (analyzed) pressure pattern is shown in panel f.

#### 4.3.13 Initial TC size and influence on subsequent intensity change

In a recent study by Carrasco et al. (2014) tropical cyclone size in the Atlantic Basin was analysed from the past two decades (1990–2010) and the connection, if any, between their size and their ability to subsequently undergo rapid intensification (RI). Three different parameters were chosen to define the size of a tropical cyclone: radius of maximum wind (RMW), the average 34-knot radius (AR34), and the radius of the outermost closed isobar (ROCI). The data for the study, came from the North Atlantic hurricane database second generation (HURDAT2), as well as the extended best track dataset, were organized into 24-h intervals of either RI or slow intensification/constant intensity periods (non-RI periods). Each interval was defined by the intensity (maximum sustained surface wind speed), RMW, AR34, and ROCI at the beginning of a defined period and the change of intensity during the subsequent 24-h period. Results indicated

that the ability to undergo RI shows significant sensitivity to initial size. Comparisons between RI and non-RI cases confirm that tropical cyclones that undergo RI are more likely to be smaller initially than those that do not. Analyses also showed that the RMW and AR34 have the strongest negative correlation with the change of intensity. When analyzing scatterplots of the data, there is a general maximum size threshold for RMW and AR34, above which RI is extremely rare. In contrast, the overall size of the tropical cyclones, as measured by ROCI, appears to have little to no relationship with subsequent intensification. The results of their work suggest that intensity forecasts and RI predictions in particular may be aided by the use of the initial size as measured by RMW and AR34.

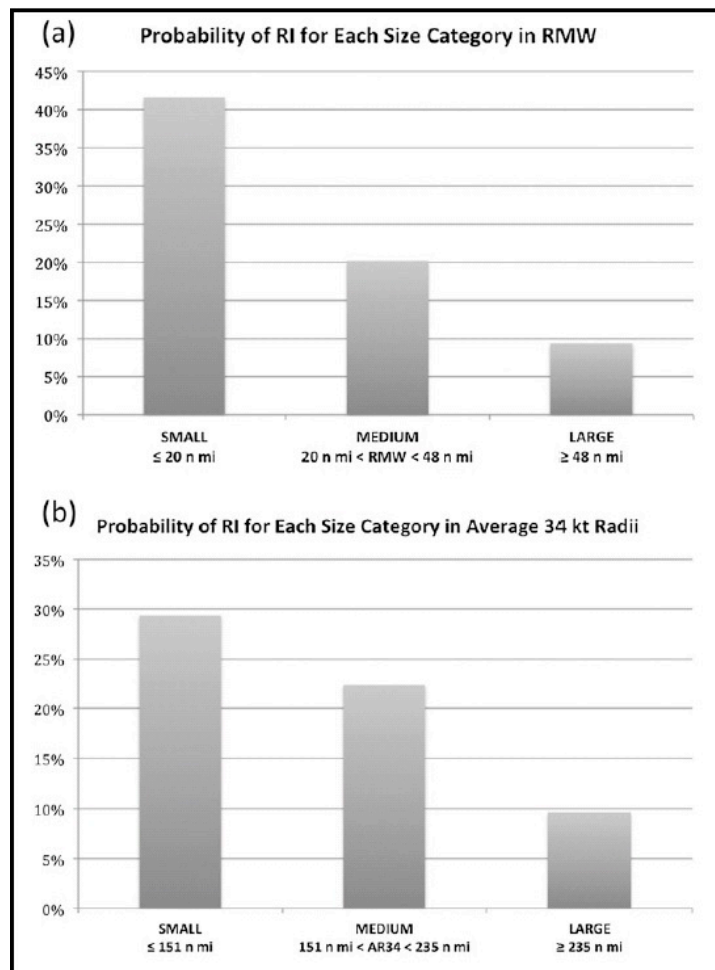


Figure 24. Probabilities for rapid intensification (RI) for three storm size categories as defined by radius of maximum winds (RMW) and average radius of gale-force (34-kt) winds in nautical miles

#### 4.3.14 Influence of environmental humidity on TC size

Tropical cyclones (TCs) are observed to span a large range of sizes; these differences are evident in the size of the eye as well as in the lateral extent of the wind, cloud, and precipitation fields. Previous studies have demonstrated that the size of a TC wind field can vary with ocean basin, time of year, latitude, minimum central pressure, stage of development, and environmental pressure (Atkinson 1971; Frank and Gray 1980; Merrill 1984; Cocks and Gray 2002; Kimball and Mulekar 2004).

The size of a TC has obvious connections with TC impacts, including storm surge, precipitation amount, area impacted by damaging winds, and the area threatened by tornadoes subsequent to landfall. Nevertheless, few studies have examined the physical mechanisms that determine TC size. Merrill (1984) hypothesized that changes in the TC size were related to angular momentum imports resulting from latitudinal changes or changes in synoptic environment. Emanuel (1986) and Rotunno and Emanuel (1987) highlighted the size of the initial disturbance as a determining factor. A study by Kimball (2006) found that model TCs initialized within a larger envelope of moisture developed into larger storms relative to those initialized within a smaller moist envelope, although the physical mechanism responsible for this difference in size was not investigated.

In a study by Lackmann and Hill (2009) it was hypothesized that the size of a TC is related to the intensity and coverage of precipitation outside the radius of maximum wind (RMW), which is in turn related to environmental relative humidity. Heavier precipitation in spiral bands outside the RMW favours a larger lateral extent of the wind field.

The hypothesis was tested using a series of idealized TC simulations in which the environmental relative humidity was varied. Dry initial environments tend to inhibit precipitation in outer portions of the TC, which should result in a narrower region of deep convection and smaller RMW, whereas more moist environments are conducive to greater precipitation at larger radii, a broader area of deep convective clouds, and larger lateral extent of the TC wind field. It was recognized that the lateral precipitation distribution can be sensitive to other factors besides environmental relative humidity, such as frontal or trough interactions and topographic forcing. However, changing the environmental relative humidity in idealized simulations provided a straightforward means of testing the primary hypothesis.

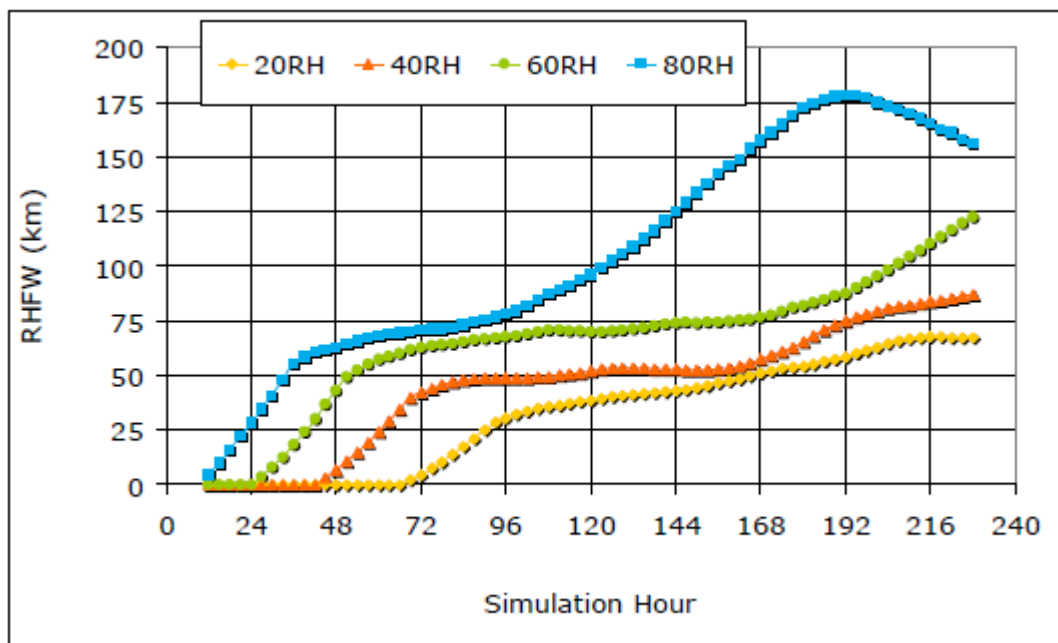


Figure 25. Evolution of the radius of hurricane-force winds (at 10 m) from various model simulations of a tropical cyclone with different initial conditions for environmental relative humidity

## References

- Black, M. L., and H. E. Willoughby, 1992: The concentric eyewall cycle of Hurricane Gilbert, *Mon. Wea. Rev.*, **120**, 947-957.
- Chen, H and S.G. Gopalakrishnan, 2014: A Study on the Asymmetric Rapid Intensification of Hurricane Earl (2010) using the HWRF System. Submitted to *J. Atmos. Sci.*
- Epstein, E. S., 1969: Stochastic dynamic prediction. *Tellus*, **21**, 739-759.
- Fujibe, F., and N. Kitabatake, 2007: Classification of surface wind fields of tropical cyclones at landfall on the Japan main islands. *J. Meteor. Soc. Japan*, **85**, 747–765.
- Grams, C.M., Wernli, H., Böttcher, M., Campa, J., Corsmeier, U., Jones, S.C., Keller, J.H., Lenz C.-J. and Wiegand, L., 2011. The key role of diabatic processes in modifying the upper-tropospheric wave guide: a North Atlantic case-study. *Q. J. R. Meteorol. Soc.* **137**: 2174–2193. DOI:10.1002/qj.891.
- Houze, R. A., S. S. Chen, B. F. Smull, W.-C. Lee, and M. M. Bell, 2007: Hurricane intensity and eyewall replacement. *Science*, **315**, 1235-1239.
- Huang, H.-L., M.-J. Yang, and C.-H. Sui, 2014: Water budget and precipitation efficiency of Typhoon Morakot (2009). *J. Atmos. Sci.*, **71**, 112–129.
- Keller, J. H., Jones, S.C. And Harr, P.A., 2014: An Eddy Kinetic Energy View of Physical and Dynamical Processes in Distinct Forecast Scenarios for the Extratropical Transition of Two Tropical Cyclones. *Mon. Wea. Rev.*, **142**, 2751–2771. doi: <http://dx.doi.org/10.1175/MWR-D-13-00219.1>.
- Kieu, C., V. Tallapragada and W. Hoggsett, 2014: Vertical structure of tropical cyclones at onset of the rapid intensification in the HWRF model. *Geophysical Research Letters*; Volume 41, Issue 9, 16 May 2014, Pages: 3298–3306.
- Kitabatake, N. 2011: Climatology of Extratropical Transition of Tropical Cyclones in the Western North Pacific Defined by Using Cyclone Phase Space. *Journal of the Meteorological Society of Japan* **89**:4, 309-325
- Kitabatake, N. and F. Fujibe, 2009: Relationship between Surface Wind Fields and Three-Dimensional Structures of Tropical Cyclones Landfalling in the Main Islands of Japan. *Journal of the Meteorological Society of Japan*, Vol. 87, No. 6, pp. 959--977, DOI:10.2151/jmsj.87.959.
- Lang, S.T.K, Jones, S.C., Leutbecher, M., Peng, M.S., Reynolds, C.A. 2012: Sensitivity, Structure, and Dynamics of Singular Vectors Associated with Hurricane Helene (2006). *J. Atmos. Sci.*, **69**, 675–694. doi: <http://dx.doi.org/10.1175/JAS-D-11-048.1>
- Liu, C., Q. Xiao, and B. Wang, 2008: An ensemble-based four-dimensional variational data assimilation scheme. Part I: Technical formulation and preliminary test. *Mon. Wea. Rev.*, **136**, 3363-3373.
- Loridan, T., E. Scherer, M. Dixon, E. Bellone and S. Khare, 2014a: Cyclone wind field asymmetries during extratropical transition in the western North Pacific. *Journal of Applied Meteorology and Climatology*, **53**, 421–428. doi: <http://dx.doi.org/10.1175/JAMC-D-13-0257.1>
- Loridan, T., S. Khare, E. Scherer, M. Dixon, E. Bellone and, 2014b: Parametric modeling of transitioning cyclone's wind fields for risk assessment studies in the western North Pacific. *Journal of Applied Meteorology and Climatology* (accepted with major revisions).
- Murnane, R. J. and J. B. Elsner (2012), Maximum wind speeds and US hurricane losses, *Geophys. Res. Lett.*, Volume 39, Issue 16
- Pantillon, F. , Chaboureau, J.-P. and Richard, E. 2014. Impact of Hurricane Nadine on the predictability of severe weather in the Mediterranean. EGU General Assembly 2014 Vienna.

- Pielke, Jr., R. A., Gratz, J., Landsea, C. W., Collins, D., Saunders, M. A., and Musulin, R., 2008. Normalized Hurricane Damages in the United States: 1900-2005. *Natural Hazards Review*, Volume 9, Issue 1, pp. 29-42.
- Poterjoy, J. and F. Zhang, 2011: Dynamics and structure of forecast error covariance in the core of a developing hurricane. *J. Atmos. Sci.*, **68**, 1586-1606.
- Poterjoy, J. and F. Zhang, 2014a: Tropical cyclogenesis predictability examined through ensemble analyses and forecasts for Hurricane Karl (2010) during PREDICT. *J. Atmos. Sci.*, **71**, 1260-1275.
- Poterjoy, J. and F. Zhang, 2014b: Inter-comparison and coupling of ensemble and variational data assimilation approaches for the analysis and forecasting of Hurricane Karl (2010). *Mon. Wea. Rev.*, **142**, 3347-3364.
- Poterjoy, J. and F. Zhang, 2014c: Systematic comparison of tangent-linear and ensemble-based four-dimensional data assimilation methods using hybrid background error covariance: E4DVar versus 4DEnVar. *Mon. Wea. Rev.*, Submitted.
- Poterjoy, J., F. Zhang, and Y. Weng, 2014: The effects of sampling errors on the EnKF assimilation of inner-core hurricane observations. *Mon. Wea. Rev.*, **142**, 1609-1630.
- Powell, M.D. and T. A. Reinhold, 2007 : "Tropical Cyclone Destructive Potential by Integrated Kinetic Energy.", *Bull. Amer. Meteor. Soc.*, vol. 88 no. 4, pp.513-526.
- Saha and Co-authors, 2010: The NCEP climate forecast system reanalysis. *Bull. Amer. Meteor. Soc.*, 91, 1015–1057.. Doi: 10.1175/2010Bams3001.1.
- Tallapragada V, Kieu C, Kwon Y, Trahan S, Liu Q, Zhang Z, Kwon I, 2013: Evaluation of storm structure from the operational HWRF model during 2012 implementation. *Mon Weather Rev.* doi:10.1175/MWR-D-13-00010.1.
- Tallapragada and Kieu, 2014: Real-Time Forecasts of Typhoon Rapid Intensification in the North Western Pacific Basin with the NCEP Operational HWRF Model. *Tropical Cyclone Research and Review*, 2014, 3(2): 63-77.
- Tallapragada, V., S. Trahan, Y. C. Kwon, Z. Zhang, C. Kieu, Q. Liu, W. Wang, M. Tong, D. Sheinin, E. Liu, B. Zhang, S. Gopalakrishnan, X. Zhang, L. R. Bernardet, R. M. Yablonsky, J. W. Bao, R. J. Pasch, J. L. Franklin, D. A. Zelinsky, B. Strahl, W. Lapenta, R. L. Gall, and F. Toepfer, 2014: Significant Advances to the NCEP Operational HWRF Modeling System for Improved Hurricane Forecasts. AMS 31<sup>st</sup> Conference on Hurricanes and Tropical Meteorology, 14.D1, San Diego, CA.
- Vigh, J. L., 2010: Formation of the hurricane eye. Ph.D. dissertation, Colorado State University, 538 pp., [Available online at <http://hdl.handle.net/10217/39054>].
- Vigh, J. L., J. A. Knaff, and W. H. Schubert, 2012: A climatology of hurricane eye formation. *Mon. Wea. Rev.*, 140, 1405–1426, doi:10.1175/MWR-D-11-00108.1.
- Vigh, J. L. and C. M. Rozoff, 2012: Impact of inner core tropical cyclone structure on the potential for rapid intensification. Extended Abstract, 30th Conf. on Hurricanes and Tropical Meteorology, Ponte Vedra Beach, FL, Amer. Meteor. Soc., Paper 8B.2, [Available online at [http://ams.confex.com/ams/30Hurricane/webprogram/Manuscript/Paper205194/vigh\\_rozoff2012\\_extended\\_abstract.pdf](http://ams.confex.com/ams/30Hurricane/webprogram/Manuscript/Paper205194/vigh_rozoff2012_extended_abstract.pdf)].
- Vigh, J. L., 2014: Development of an HWRF diagnostics module to diagnose intensity and structure using synthetic flight paths through tropical cyclones. Final report to the Development Testbed Center Visitor Program, 44 pp., Boulder, CO.

- Vigh, J. L., C. Kieu, V. Tallapragada, L. R. Bernardet, and E. W. Uhlhorn, 2014: Use of synthetic profiles to diagnose simulated tropical cyclones in regional hurricane models. Extended Abstract, 31st Conf. on Hurricanes and Tropical Meteorology, San Diego, CA, Amer. Meteor. Soc., Paper 16D.6, [Available online at [https://ams.confex.com/ams/31Hurr/webprogram/Manuscript/Paper244834/vigh\\_etal\\_2014\\_preprint\\_31hurr.pdf](https://ams.confex.com/ams/31Hurr/webprogram/Manuscript/Paper244834/vigh_etal_2014_preprint_31hurr.pdf)].
- Wang, Y., 2009: How do outer spiral rainbands affect tropical cyclone structure and intensity? *J. Atmos. Sci.*, **66**, 1250–1273.
- Weng, Y. and F. Zhang, 2011: Airborne doppler radar observations assimilation with an ensemble kalman filter for hurricane initialization and prediction: Katrina (2005). *Mon. Wea. Rev.*, Accepted.
- Yang, M.-J., D.-L. Zhang, X.-D. Tang, and Y. Zhang, 2011a: A modeling study of Typhoon Nari (2001) at landfall. 2: Structural changes and terrain-induced asymmetries. *J. Geophys. Res.*, **116**, D09112.
- Zhang, F., Y. Weng, J. Sippel, Z. Meng, and C. Bishop, 2009: Cloud-resolving hurricane initialization and prediction through assimilation of Doppler radar observations with an ensemble Kalman filter. *Mon. Wea. Rev.*, **137**, 2105-2125.
-